RSC Advances

ROYAL SOCIETY OF CHEMISTRY

www.rsc.org/advances

Low Temperature, Shape-selective Formation of Sb_2Te_3 Nanomaterials and their Thermoelectric Applications

U. Nithiyanantham,[$] Sivasankara Rao Ede,[$] M. Fevzi Ozaydin,[#] Hong Liang[#] A. Rathishkumar[@] and Subrata Kundu*[$]

[$]Electrochemical Materials Science (ECMS) Division, [@] Central Instrumental Facility (CIF) Division, CSIR-Central Electrochemical Research Institute (CECRI), Karaikudi-630006, Tamil Nadu, INDIA.

[#]Materials Science and Mechanical Engineering, Texas A&M University, College Station, TX 77843-3123, USA.

* To whom correspondence should be addressed, *E-mail: skundu@cecri.res.in; kundu.subrata@gmail.com,* Phone: (+ 91) 4565-241487, FAX: +91-4565-227651.

ABSTRACT

Shape-selective Sb_2Te_3 nanomaterials have been synthesized utilizing a simple wet-chemical route at a low temperature within a short time. Dumb-bell like and chain-like Sb_2Te_3 nanomaterials are formed by the reaction of Te metal powder with $SbCl_3$ salt in the presence of alkaline 2,7-DHN in CTAB micelle media at 80 °C temperature. The size and shape of nanomaterials can be easily tuned by changing the molar ratio of the surfactant to metal salts and controlling the other reaction parameters. The middle part of the dumb-bell like shapes are ~ 15 ± 1 nm, and the length ~ 50 ± 7 nm while the diameter of the chains is ~ 125 ± 7 nm. The opto-electronic property, thermal stability and specific growth mechanism for the formation of different shapes are elaborated in detail. Both the morphologies have been tested for thermoelectric applications. Among the two different morphologies, the chain- like morphology gives better thermoelectric figure of merit (ZT) value compared to dumb-bell like morphology at 300K. The increase in ZT value of chain-like morphology is due to reduction of the lattice thermal conductivity via the effective phonon scattering that present at the interface between boundaries of the nanograins and in the rough surfaces of the nano-chains. The maximum ZT temperature moves significantly to the high temperature zone indicating that the shape-selective Sb_2Te_3 nanomaterials have potential application in power generation.

Introduction

The conversion of thermal energy to electrical energy is known as thermoelectric (TE) conversion. The TE effect is useful for power generation and refrigeration according to the Seebeck and Peltier effects which are expected to play a demanding role in solving the energy crisis in the future. Nowadays, the world's demand for energy is increasing day by day and the environmental impact of global climate change due to the combustion of fossil fuels is becoming increasingly alarming. The best way to sustain our electricity needs is via scavenging the waste heat by nanoelectric generator. A TE generator can convert an enormous amount of waste heat to electricity from home heating, automotive exhaust and from industrial processes. A TE generator is a solid state electronic device which is silent, reliable, scalable, having no moving part that makes them ideal for small distributed power generation.[1] The TE technology can be useful in different fields including solar heat utilization, waste heat recovery, temperature controlled seats, portable picnic coolers and in micro-processors.[2] The advantage over the synthesis of TE materials is conversion of waste heat energy into electrical energy and the current research technology focused based on increment of the ZT value of TE materials. A thermoelectric generator consists of two thermoelectric semiconductors (n-type and p-type) subjected to a temperature difference, $T_{hot} - T_{cold}$, and electrically connected in series. In the n-type semiconductor, most charge carriers are negatively charged electrons, whereas in the other one most of the carriers are positively charged holes. In a temperature gradient, electrons and holes tend to accumulate on the cold side. An electric field E develops between the cold side and the hot side of each material, which gives a voltage when integrated over the length of each. The voltages of the n- and p-type semiconductors add up and drive an electrical current through an electrical load. The product of the voltage and the current is the electrical power output of the generator. According the Fourier's law, thermal conduction of the thermoelectric materials add thermal path from hot end to cold end which is decrease the some of the heat energy and reduces the efficiency. Usually, for all heat engines cannot exceed Carnot limit, $\eta_{max} = (T_H-T_C)/T_H$, where T_H and T_C are the temperatures of the hot and the cold side of the devicerespectively.[3] The Seebeck coefficient, electrical resistivity, thermal conductivity and ZT values are depend up on the nature of materials. The efficiency of power generated by TE material is also depends on the how much heat is provided at the hot end. The good TE material obtained high σ and low κ, characteristics indicative of a so-called phonon-glass/electron-crystal (PGEC) and in general, the low-dimensional materials gives better PGEC performance.[4] The material, which

is having high TE properties are interrelated with S, σ and k and the efficiency was improved via the power factor $S^2\sigma$ through electronic doping and modifying the band structure.[5] The physical properties of TE materials mainly depend on the purity of synthesized nanomaterials as the impurity of the materials will affect the concentration of charge carriers and conducting prosperities.

The efficiency of TE materials has been calculated using the dimensionless figure of merit (ZT) where

$$\mathbf{ZT} = \frac{\mathbf{S^2\sigma}}{\boldsymbol{\kappa}} \times \mathbf{T}$$

where, S is the Seebeck coefficient, σ is the electrical conductivity, κ is the thermal conductivity and T is the absolute temperature.[6] The increasing of ZT value thermoelectric materials lies in achieving simultaneously high electronic conductivity (s), high Seebeck coefficient (S) and low thermal conductivity (k) in the same material. The thermal conductivity κ has a contribution from lattice vibrations, κ_{latt}, called the lattice thermal conductivity. Thus, $\kappa = \kappa_{el} + \kappa_{latt}$, where κ_{el} is the carrier thermal conductivity. Intuitively, the thermal conductivity must be low as a large temperature difference (ΔT) must be maintained; a large thermal conductivity will short the thermal circuit. It is possible to visualize two approaches aimed to increase ZT: either the power factor is maximized or the thermal conductivity is minimized. An effective way to maximize the figure of merit (ZT) is to manipulate the lattice thermal conductivity, which is the only parameter not determined by the electronic structure. All other material parameters, such as electrical conductivity and thermoelectric power, are correlated with the electronic structure of the material and thus, in most cases, cannot be optimized independently. The classical kinetic theory provides a good approximation for the lattice thermal conductivity: $\kappa_{latt} = 1/3C_v l v_s$, where C_v is the specific heat at constant volume, l is free phonon path, and v_s is the average velocity of sound.[7] At very low temperatures (under 40 K), the behaviour of κ_{latt} is dominated by the Debye T^3 law for C_v. Phonon scattering is insignificant in this temperature range, because of the low number of excited phonons and their very long wavelength. However, at high temperatures, that is, above the Debye temperature, C_v approaches the classical value of 3R, making κ_{latt} primarily depend on l which is determined by phonon–phonon scattering. From past few years, a vast study is being carried out on how to increase the ZT value for potential TE applications. The theoretical calculations and experimental investigation speaks that the decreasing the dimension and size of the building blocks of TE materials are the efficient and

promising ways to improve ZT values. Pnictogen chalcogenides (group V - VI, especially the $V_2 – VI_3$ type) and their different alloys are well suited for realizing high ZT due to their low band gaps, complex crystal structure and the presence of heavy elements.[8] Theoretical calculations[9] says that the ZT value of Bi_2Te_3 can be attained to 5 while the observed ZT values of Bi_2Te_3/Sb_2Te_3 super lattices at room temperature (RT),[10] Bi_2Te_3/Sb_2Te_3 bulk nanocomposites at 450 K[11] and bismuth antimony telluride bulk alloy at 373 K[12] are 2.4, 1.47 and 1.4 respectively.

Among the different narrow band gap semiconductor materials having tetradymite structure, antimony telluride (Sb_2Te_3) having the space group R_{3m} found practical interest due to superior thermoelectric characteristics near RT and used widely in TE devices.[10,13] Sb_2Te_3 single crystal has great attention for σ (3.13 - 5.26) × 10^5 Ω^{-1} m^{-1} at 300 K and low K (1.6 – 5.6) W m^{-1} k^{-1} at 300 K whereas the S value is low ~ 83-92 μV k^{-1} at 300 K.[14] To get high ZT, it has to have high σ value and low k value. The S value can be reached higher by introducing nanostructures. It is very difficult to attain high σ for nanomaterials without any specific shape although theoretical study predicted very high ZT value of nanomaterials. Sb_2Te_3 thin films or nanostructures can be fabricated using variety of routes such as metal organic chemical vapour deposition,[15] molecular beam epitaxy,[16] sputtering,[17] evaporation,[18-20] hydrothermal synthesis,[21-23] electro chemical atomic layer epitaxy,[24] vapour-liquid-solid-growth,[25] solvothermal approach,[26] electrochemical deposition[27] and single source precursor.[28] Generally template based synthesis route are less expensive and easy to perform. Jin et al. synthesized template based Sb_2Te_3 nanowires arrays in PAAM template.[27] Dong et al. prepared Sb_2Te_3 nanobelts by spark plasma sintering at 200 °C.[29] Pinisetty et al. fabricated Sb_2Te_3 nanowire or nanotubes using electro deposition techniques.[30] Shi et al. prepared Sb_2Te_3 nanobelts under inert atmosphere using hydrothermal route.[21] Most of the above reports focused on the fabrication and characterization of Sb_2Te_3 thin films but less attention is given for the colloidal synthesis at low temperature, study on different optical and electronic properties and detailed study on their TE properties. Moreover, most of the previous reports utilized long reaction time, high temperatures and reaction took place at inert atmosphere. Besides, the final product contained mixed shaped particles and elemental Te as impurity. As Te is a metalloid and contains free electrons, it may neutralize the positive holes of the P-type Sb_2Te_3 and decrease the σ and $S^2\sigma$.[31] Attaining low value of σ is the major problem in TE nanostructures. Nowadays, the shape-selective synthesis of metal and metal oxide nanomaterials has been reported frequently as the properties of the nanomaterials can

be changed with the change in shapes. Kundu et al. reported shape-selective metal and metal oxide nanomaterials such as Au,[32] Ag,[33] Os,[34] cobalt oxide,[35] TiO_2 [36] for different important application purposes. In this study, we prepared shape-selective Sb_2Te_3 nanocrystals at low temperature within a short reaction time. To the best of our knowledge, there are no reports on the detailed optical, electronic properties of dumb-bell and chain-like Sb_2Te_3 nanomaterials synthesized at low temperature within a short reaction time and their detailed study on TE properties with the change in particle's morphology.

Herein, we report for the first time, the synthesis of shape-selective Sb_2Te_3 nanomaterials of low temperature within a short reaction time. Sb_2Te_3 nanomaterials are formed by the reaction of Te metal with $SbCl_3$ salt with alkaline 2,7 di-hydroxynapthalene (2,7-DHN) in CTAB (cetyltrimethyl ammonium bromide) micelle media. The dumb-bell like and chain-like morphology has been formed just by tuning the metal salt to CTAB molar ratio and controlling other reaction parameters. The average size at the middle part of the dumb-bell like shapes are ~ 15 ± 1 nm and the length of ~ 50 ± 7 nm and the nominal length of connected dumb-bell like particles is ~ 130 ± 5 nm. The average diameter of the chain-like Sb_2Te_3 nanomaterials is ~ 125 ± 7 nm and the nominal length of the chains is ~ 1.2 - 1.5 µm. Both the morphology has been used as potential TE material and among two morphologies the chain-like morphology showing better ZT value compare to dumb-bell-like morphology at 300K. The present synthesis process is simple, cost-effective, robust and takes place at low temperature with very high product selectivity and might be vastly applied in future energy related applications.

Experimental part

Reagents and Instruments.

Cetyl trimethyl ammonium bromide (CTAB, 99%), 2,7-dihydroxynaphthalene (2,7-DHN), antimony trichloride ($SbCl_3$), Te metal powder, sodium hydroxide (NaOH), Di-ethylene glycol (DEG) are analytical reagent grade, purchased from Sigma-Aldrich, India and used as received. Graphite die and graphite sheet were purchased from Sigma-Aldrich, USA and used as received. De-ionized (DI) water was used for the entire synthesis process. The synthesized Sb_2Te_3 nanomaterials were characterized with several spectroscopic and microscopic techniques like UV-Vis, TEM, FE-SEM, EDS, XRD, thermal analysis and FT-

IR analyses and the detailed specification of the instruments are given in online supporting information (SI) section.

Low-temperature, shape-selective formation of Sb_2Te_3 nanomaterials.

Sb_2Te_3 nanomaterials are synthesized by the reaction $SbCl_3$ salt with Te metal powder under alkaline condition in CTAB micelle media. In a typical synthesis, 20 mL of DEG was mixed with 10 mL of 0.5 (M) NaOH solutions and stirred the mixture for 10 min. Then 0.6 mg of Te metal powder was added in the solution mixture and stirred well with heating at 60-70 °C. The resultant solution was cement colour at this stage. Then 0.1 g of 2,7-DHN was added at once while stirring condition then the solution colour turned light bluish. After some time, the light blue colour became dark and stirring was continued for another 30 min. Then 10 mL of CTAB solution (10^{-1} M, stock solution) was added, stirred for 10 min and finally 10 mL of DEG solution containing 0.5 gm of $SbCl_3$ salt was added and stirred well. Heating and stirring was continued for another 30 min. Then, the resultant solution color became whitish black. After 30 min reaction was stopped, precipitate was washed with water and ethanol several times and dried the solid mass at 80 °C in vacuum for 6 hrs. The sample exclusively contains Sb_2Te_3 nanomaterials having dumb-bell like morphology. Other morphology was also prepared by changing the concentration ratio of CTAB to precursor metal salts. Table 1 shows the final concentration of all the reagents used, reaction time, size and shape of the Sb_2Te_3 nanomaterials formed. It is important to mentioned here that the final concentrations of all reagents are different from initial concentrations. Initially, we prepared stock solutions with particular concentration and while synthesizing the nanomaterials, different amounts of stock solutions or reagents are mixed with each other at a certain ratio and calculated the concentration of individual reagents in the total solution mixture which named as 'final concentrations' of reagents. Moreover, it must mentioned here that some other intermediate concentrations of CTAB, Sb_2Te_3 nanomaterials were formed but not any specific shape rather mixture of different shapes. The step-wise formations of the Sb_2Te_3 nanomaterials are schematically shown in Scheme 1.

Fabrication of Sb_2Te_3 nanomaterials by spark plasma sintering method for thermoelectric meassurment.

The polycrystalline samples of Sb_2Te_3 with the nominal compositions were utlized for the ZT (ZT, Z figure of merit and T absolute temperature) analysis. The synthesized material used in various ways for TE sample preparation as discussed herewith. Initially, cylindrical

graphite die was used for spark plasma sintering presses. The die was lined with graphite sheet to facilitate easy removal of the sintered specimen. Same amount of each Sb_2Te_3 sample was weighed and placed in the die and then sintered at 275 °C under uniaxial pressure of 40 MPa for 5 min. Sintering temperature depends on the phase diagrams Sb_2Te_3 alloys. TE measurement was always done below the sintering temperature. High DC current was passed between graphite electrodes and axial pressure was applied simultaneously from the beginning of the sintering cycle. The sample was heated by the Joule-heating and the sparking that leads to the faster heat and mass transfer instantaneously. After the sintering, the power was turned off and the sample was allowed to cool. Each sample was ground on both sides and placed in acetone to remove the leftover graphite sheet completely for the measurements.

Laser flash method was used to determined the thermal diffusivity by using Flash line 3000 system by Anter Corporation. Radiation source was high speed Xenon lamp-pulse with pulse width of 400 μs to 600 μs. The given pulse energy was up to 15J and thermal diffusivity range was 0.01 to 1000 mm^2/s in Argon atmosphere and the temperature range is RT to 1000 °C. The xenon lamp flash method was used to measure thermal diffusivity at a designated temperature. At this temperature the sample bottom was irradiated with a programmed energy pulse. This energy pulse resulted in a homogeneous temperature rise at the sample top. The resulting temperature rose on the top surface of the sample was measured by a high speed IR (infra-red) detector and thermal diffusivity values were computed from the temperature rise versus time data. In this methodology, one side of a sample with a defined thickness was heated using a short light pulse and the resulting increase in temperature on the other side was detected via contactless, infrared detector method.

Heat capacity was measured using Modulated DSC (MDSC) methodology. The guideline principal of modulated DSC is applying two heating rates simultaneously and measuring how they would affect the rate of heat flow. As compared to standard DSC, modulated heating rate allowed the measurement of both the heat flow that responded to heating rate (reversing signal) and the heat flow that responded to absolute temperature/time (non-reversing signal). Heat capacity (C_p) is contained in the reversing signal and given as:

$$\text{Rev } C_p = \frac{\text{Heat flow amplitude}}{\text{Heating rate amplitude}} \times K\,(C_p\ \text{Rev})$$

Where, K C_p Rev = Calibration constant for reversing C_p. Finally, the bulk density was measured using standard Archimedes method. The total time for each sample was approximately 72h excluding equipment downtime for repair and other usage.

Preparation of sample for other optical, spectroscopy and microscopic characterization.

The shape-selective Sb_2Te_3 nanomaterials were characterized using UV-Vis, TEM, FE-SEM, EDS, XRD, XPS, thermal analyses and FT-IR studies. The Sb_2Te_3 nanomaterials are prepared after successive centrifugation and drying. For UV-Vis spectroscopic analysis, a small amount of solid sample was taken, sonicated with DI water and the aqueous dispersion was used for the analysis. The solid Sb_2Te_3 powder was mixed with DI water, sonicated for 30 min and used for TEM sample preparation and other thin films preparation. The samples for TEM were prepared by placing a drop of the corresponding Sb_2Te_3 nanomaterials suspension onto a carbon coated Cu grid followed by slow evaporation of solvent at ambient conditions. For EDS, XRD and FT-IR analysis, glass slides were used as substrates for thin film preparation. The glass slides were cleaned thoroughly in acetone and sonicated for about 30 min. The cleaned substrates were covered with the Sb_2Te_3 nanomaterials suspension and dried in air. After the first layer was deposited, subsequent layers were deposited by repeatedly adding more Sb_2Te_3 nanomaterials suspension and drying. Final samples were obtained after 4-5 times depositions and then analyzed using the above techniques. For FE-SEM, the sample was prepared by the same drop casting route over glass slide but a low concentration was used unlike XRD, FT-IR. For XPS and TGA/DTA analysis, the as prepared Sb_2Te_3 nano powders were directly used for the measurement. The sample preparations for thermoelectric ZT measurement are discussed before in previous section.

Results and Discussion

Transmission Electron Microscopy (TEM) and Field Emission Scanning Electron Microscopy (FE-SEM) analysis.

Shape-selective Sb_2Te_3 nanomaterials are synthesized by the reaction of $SbCl_3$ salt with Te metal powder in presence of alkaline 2,7-DHN in CTAB micelle media under two hrs of heating and stirring at 80 °C. Figure 1, A-C are the TEM images of the Sb_2Te_3 nanomatrials having dumb-bell like shape at different magnification. A and B are the images at low magnification where C is the image at higher magnification. After analysis of the images, the average size at the middle part of the dumb-bell like shapes are ~ 15 ± 1 nm and

the length of ~ 50 ± 7 nm and the nominal length of connected dumb-bell like particles is ~ 130 ± 5 nm. In most of the cases, the dumb-bell like particles are separated from one another. However, in few cases they are connected together. The inset of Figure 1C shows the corresponding selected area electron diffraction (SAED) pattern which says that the particles are crystalline in nature. Figure 1, D-F are the TEM images of the Sb_2Te_3 nanomaterials having chain-like morphology at different magnification. Image D and E are at the low magnification where image F shows at higher magnification. From the images, we can see that all the Sb_2Te_3 nanomaterials are interconnected each other and generated the chain-like morphology. The average diameter of the chain-like Sb_2Te_3 nanomaterials is ~ 125 ± 7 nm and the nominal length of the chains is ~ 1.2 - 1.5 µm. The chain-like morphology are formed either by the rational interconnection of spherical Sb_2Te_3 particles or by the temperature induced fusion of spherical Sb_2Te_3 particles. The inset of Figure 1F shows the corresponding SAED pattern which is a continuous ring type pattern indicates the particles are crystalline in nature. Figure 2 shows the FE-SEM images of the Sb_2Te_3 nanomaterials for two different morphologies of the dumb-bell like and chain-like shapes. Figure 2, A and B shows the FE-SEM image of the dumb-bell like shape whereas Figure 2, C-D shows the FE-SEM image having chain-like shape. From the image, it is seen that the dumb-bell like morphology are aggregates each other that might be due to deposition of higher concentration of sample during sample fabrication and drying. The chain-like morphology is clearly visible and the size of the both morphology are matches with the TEM results as discussed before. The average lengths of the Sb_2Te_3 chains are calculated by the FE-SEM images which are of the order of a micron. Hence, from the overall morphological analysis, we have confirmed that two distinct morphologies of dumb-bell like and chain-like nanomaterials were successfully synthesized by tuning the reaction parameters during the synthesis process.

UV-Visible (UV-Vis) spectroscopic, energy dispersive X-ray spectroscopic (EDS) and thermal analysis study.

Figure S-1 (online SI section) shows the UV-Vis absorption spectra of the reaction mixtures at different stages of the synthesis process. The absorption spectra of two different Sb_2Te_3 nanomaterials solution having dumb-bell like and chain-like morphology did not show any specific absorption band. Moreover, as there are no reports of the UV-Vis spectra of Sb_2Te_3 nanomaterial, we are unable to compare our electronic spectra with previous literature. The detailed UV-Vis analysis at the different stages of synthesis process is given in

online SI section. Figure S-2 (online SI section) is the result obtained from the energy dispersive X-ray spectroscopic (EDS) analysis which is used to identify the probable elements present in the synthesized product and the spectrum consisted of the different peaks for Sb, Te, C, O, Cl and Br. Similar types of EDS spectral analyses were reported earlier by Dong et al.[29] and Shi et al.[21] for their synthesis of Sb_2Te_3 nanomaterials. The detailed EDS analysis was given in online SI section. Figure S-3 (online SI section) is the combined thermogravimetric analysis (TGA) and differential thermal analysis (DTA) of the as-synthesized Sb_2Te_3 nanomaterials on CTAB micellar media where we used dumb-bell like morphology for entire TGA-DTA analysis. In TGA analysis, we have started our experiment with 5.82 mg of sample and after heating up to 1000 °C, the amount of sample remained was 3.28 mg which indicates the % of weight loss is 43.6%. From the DTA curve there is no noticeable change was observed. The detailed analysis was given in online SI section.

XRD analysis.

The X-ray diffraction (XRD) patterns of the shape-selective Sb_2Te_3 nanomaterials are shown in Figure 3. In Figure 3, pattern A denotes for dumb-bell like morphology whereas pattern B is of chain-like morphology. Both the patterns gave almost identical XRD features which are quite expected as both the samples are the same Sb_2Te_3 material having difference only in their shapes. Several high and low intense diffraction peaks are originated in the 2θ range 15-70°. The observed peaks are corresponding to the diffraction from (101) planes at 23.2 degree, (014) at 25.5 degree, (015) planes at 27.6 degree, (10$\underline{10}$) plane at 38.3 degree, (01$\underline{11}$) plane at 40.5 degree, (110) plane at 43.5 degree, (00$\underline{15}$) plane at 46.0 degree, (1013) plane at 47.2 degree, (205) plane at 49.7 degree, (027) plane at 51.3 degree, (02$\underline{10}$) plane at 57 degree, (10$\underline{19}$) plane at 62.8 degree, (01$\underline{20}$) plane at 66 degree and (125) plane at 67.9 degree respectively. All the features confirmed the formation of hexagonal structure of Sb_2Te_3 nanomaterials having space group R3m (no 166) with the Joint Committee for Powder Diffraction Standard (JCPDS) file number 15-0874. Similar types of XRD pattern was reported earlier by Dong et al. for their synthesis of Sb_2Te_3 nanosheets using spark plasma sintering.[28] Shi et al. observed rhombohedral phase of Sb_2Te_3 nanomaterials having JCPDS file number 65-3678 as reported by their synthesis of nanobelts.[21] No impurity peaks such as elemental Te are detected by XRD indicating that the process was good and efficient for the formation of single phase Sb_2Te_3 nanomaterials without the formation of elemental Te. It was reported before that elemental Te was formed as an impurity together with Sb_2Te_3.[21, 26, 37] The Te impurity does not only give separate XRD peak but also reduces the carrier

concentration that gives rise to the reduced σ value and lower the $S^2\sigma$ value while TE efficiency measurements. In our process, we used CTAB as stabilizing agent and the selective interaction of CTAB with different crystal planes of Sb_2Te_3 might alter the growth rates and intensity of different crystal planes.

X-ray Photoelectron Spectroscopy (XPS) analysis.

X-ray photoelectron spectroscopy (XPS) analysis of Sb_2Te_3 nanomaterials is shown in Figure 4. Like EDS analysis, here also we used dumb-bell like morphology for XPS study although chain-like morphology is also measured which gave similar spectral feature (not shown here) which is quite expected. In Figure 4, 'A' indicate the survey spectrum and 'B-F' indicates the high resolution scan for Sb (3d) ,Te (3d), Te (4d), O (1s), and C (1s) respectively. The survey spectrum in Figure 4A contains the characteristic peak of Te (3d) at 583.3 eV, Sb (3d) at 538.3 eV, O (1s) at 529.9 eV, C (1s) at 285 eV, Te (4d) at 44.3 eV and Sb (4d) at 35.2 eV respectively. In Sb (3d) peak in Figure 4B is characterized by a doublet which arises due to spin-orbit coupling ($3d_{3/2}$ and $3d_{5/2}$). The peak positions for Sb $3d_{3/2}$ at 538.9 eV and Sb $3d_{5/2}$ are at 531.1 eV respectively. As the peak positions of Sb (3d) is very close to O (1s), during deconvolution, O (1s) peak is also plotted together with Sb (3d) peaks. Figure 4C shows the high resolution XPS spectra for Te (3d) which arises as a doublet due to spin orbit coupling of Te $3d_{3/2}$ and $3d_{5/2}$ peaks. Figure 4D shows the XPS spectrum of Te (4d) peaks which appeared at a binding energy of 44.2 eV. The O (1s) XPS spectrum is observed in Figure 4C where the peak appeared at a binding energy of 529.7 eV. As the XPS peak for $Sb3d_{5/2}$ is near to O (1s) peak, during deconvolution of O (1s) peak, both O (1s) and Sb $3d_{5/2}$ peaks are plotted together like Figure 4B. Figure 4F is the high resolution scan for carbon C (1s) where the peak came at an expected binding energy value of 285.02 eV. All the peaks for Sb (3d) and Te (3d) at specific binding energies are matching with literature reports.[28, 38]

FT-IR analysis.

The FT-IR spectra of pure CTAB and CTAB bound Sb_2Te_3 nanomaterials are shown in Figure 5. A comparison between two spectra not only confirms the presence but also reveals the nature of interaction taking place between CTAB and Sb_2Te_3 nanomaterials. Here we report the FT-IR spectrum of Sb_2Te_3 nanomaterials having dumb-bell like shape (although other morphology is also tested but not shown here as it gave almost similar feature). It is reported earlier that the FT-IR spectrum of CTAB capped metal NPs strongly depends on the

NPs shape. In Figure 5, spectrum A indicates the FT-IR spectrum of only CTAB and spectrum B indicates for CTAB bound Sb_2Te_3 nanomaterials. In both the spectra, there is no strong peak appear in the range 3450-3750 cm^{-1} which indicates, that there is no water molecule or moisture present in the sample. In case of only CTAB sample, a strong peak at 3331 cm^{-1} is appeared due to NH stretching which is absent or very weak in case of CTAB band Sb_2Te_3 indicating the strong interaction between them. For only CTAB, three other strong peaks at 3012 cm^{-1}, 2918 cm^{-1} and 2847 cm^{-1} which are due to secondary amine group stretching, C-H anti- stretching and C-H stretching respectively. All these specific peaks are either low intense or shifted in case of CTAB bound Sb_2Te_3 nanomaterials. For only CTAB, a strong peak at 1470 cm^{-1} is observed due to C-N stretching and a peak at 1129 cm^{-1} is due to N-H bending. It is reported before that the region 1300-1680 cm^{-1} is signifying due to CH_2 scissoring mode of vibration and O-H bending mode of water molecule around the bound head group. Other small intense peaks are also seen at 955 cm^{-1} and 906 cm^{-1} respectively. The peaks observed at 1129 cm^{-1} and 955 cm^{-1} are shifted to 1075 cm^{-1} and 926 cm^{-1} in the case of CTAB bound Sb_2Te_3 sample indicating the interaction between them. In curve b, in case of CTAB bound Sb_2Te_3 sample, two strong intense peaks appeared at 673 cm^{-1} and 583 cm^{-1}. Similar type of FT-IR spectrum of only CTAB is reported earlier.[36] Hence, the above FT-IR analysis confirms the attachment of CTAB on the Sb_2Te_3 nanomaterial surface most probably via the nitrogen head group of the CTAB molecule due to presence of an ammonium ion on its surface.

Mechanism for the formation of shape-selective Sb_2Te_3 nanomaterials.

The formation of shape-selective Sb_2Te_3 nanomaterials was materialized by the chemical reaction of $SbCl_3$, Te metal powder and alkaline 2,7-DHN in presence of CTAB micelle media under continuous stirring and heating at 80 °C as seen in Scheme 1. In our study, we did some control experiments to check the role of different reaction parameters. We have seen that in absence of CTAB, keeping all other reaction parameters fixed, Sb_2Te_3 was formed, but the particles are not stable and agglomerated as seen in TEM analysis (not shown here) due to absence of specific stabilizer. If the reaction is carried out without NaOH, the reaction does not form any Sb_2Te_3 nanomaterials. Moreover, the absence of 2,7-DHN, Te metal powder was not at all converted into Te^{2-} ions and there was no reaction with $SbCl_3$ and resulted no Sb_2Te_3 nanomaterials. Hence, for the formation of Sb_2Te_3 nanomaterials, a certain concentration ratio of the reagents is important to generate the specific morphology. As

discussed in experimental section, other intermediate concentrations, Sb_2Te_3 nanomaterials are formed but they formed mixture of different shapes and sometimes they aggregated with each other. Before discussing the chemical reaction takes place, we checked the pH of the solution mixture for the formation of Sb_2Te_3 nanomaterials. The pH of Te metal powder in di-ethylene glycol is 4.68, the pH of $SbCl_3$ solution in diethylene glycol solution is 1.3, pH of alkaline 2,7-DHN is 13.20, pH of all the reagents mixture is 11.85 and the pH of the Sb_2Te_3 nanomaterials after formation is 8.63 (for dumb-bell like shape) and 8.84 (for chain-like shape) respectively. In our experimental condition we believed that there is Te reduction takes place with the presence of alkaline 2,7-DHN solution as seen in equation (1-3) but there is no dismutation reaction takes place as per equation (4).

$$Te + 4OH^- \xrightarrow{80\ ^\circ C} TeO_2 + 2H_2O \quad .....(1)$$

$$TeO_2 + 2C_{10}H_8O_2 \xrightarrow{80\ ^\circ C} Te + 2C_{10}H_8O_2^{2-} + 2H_2O \quad .....(2)$$

$$Te + 2C_{10}H_8O_2 + 4OH^- \xrightarrow{80\ ^\circ C} Te^{2-} + 2C_{10}H_6O_2^{2-} + 4H_2O \quad .....(3)$$

$$Te + 6OH^- \xrightarrow{80\ ^\circ C} TeO_3^{2-} + 2Te^{2-} + 3H_2O \quad .....(4)$$

To confirm that the Te metal powder is reduced to Te^{2-} by 2,7-DHN, a highly pure Te metal powder is dissolved and heated in the presence of alkali in diethylene glycol and then 2,7 DHN solution added to it. Initially, a faint purple color was observed under continuous stirring and heating indicating the formation of Te^{2-} ions by the reduction of 2,7-DHN instead of dismutation reaction of Te. A similar type of reaction mechanism was reported earlier by dong et al. for the formation of Sb_2Te_3 nanomaterials using hydrazine hydrate as reducing agent.[25] Hence, in continuation of the reaction (1-3), the Te^{2-} ions re-attached with the CTAB surfactant due to opposite charge on CTA^+ ions by electrostatic interactions and Te^{2-} - CTA^+ complex is formed. Then, at once the DEG solution of $SbCl_3$ is added Sb^{+3} ions immediately reacted with Te^{2-} - CTA^+ and formed Sb_2Te_3 nuclei bound CTAB surfactant.

$$Te^{2-} + CTAB \xrightarrow{80\ ^\circ C} Te^{2-} + CTA^+ + Br^- \quad .....(5)$$

$$2\,Sb^{3+} + 3Te^{2-} + CTA^+ \xrightarrow{80\ ^\circ C} Sb_2Te_3 @ CTAB \quad .....(6)$$

In the above reaction, 2,7-DHN acted as a reducing agent which reduced Te metal to Te^{-2} ions while CTAB acted as a stabilizing agent. It was reported earlier by others that aromatic molecules having hydroxyl group in their benzenoid rings and other polyol compounds can act as reducing agents and can be used for the reduction of metal ions for the synthesis of metal NPs.[40-44] Many compounds having hydroxyl group such as ascorbic acid,[45] TX-100,[46] β-naphthol,[47] DNA,[48-49] 2,7-DHN[39] has been used extensively for the reduction of metal ions and the formation of metal NPs. Hence, in our present study, once the Te metal powder reduced to Te^{-2} ions, the $SbCl_3$ salt solution was added, Sb^{+3} reacted with Te^{-2} and produced Sb_2Te_3 nuclei. Then, Sb_2Te_3 nuclei were attached to CTAB surfactant and favoured the crystallization in a preferential direction. With the increase in time, the production of Sb_2Te_3 nuclei was reduced and slow crystallization allowed to forming Sb_2Te_3 nanomaterials via Ostwald ripening process. Once the small Sb_2Te_3 nuclei were formed, they started to act as seed particles and finally the CTAB adsorbed on the particular facet of the Sb_2Te_3 nanomaterials and generated the specific morphology. The formation of specific shape depends upon two factors, first one is the faceting tendency of the stabilizing agent and second one is the growth kinetics that is rate of supply of M (0) to the crystalline planes.[50] We had seen that when the concentration of CTAB was high, dumb-bell like morphology was formed while at low concentration chain-like morphology was formed. It was reported earlier that CTAB can form rod-shaped and worm-like shaped micellar templates at higher concentrations (~ 10^{-1} - 10^{-2} M).[51,52] So we believed that at a higher concentration of CTAB, the Sb_2Te_3 nuclei grown over those templates and generated the dumb-bell like morphology. While at low CTAB concentration, they present as a mixture of free surfactant and micelles and the particles had grown without any restriction and generated the spherical Sb_2Te_3 particles initially, which then aggregated during heating and formed the chain-like Sb_2Te_3 nanomaterials. The TEM and FE-SEM analysis in Figure 2 and Figure 3 clearly indicates that the formation of both morphologies was near to 100% and no other shapes are mixed with the synthesized nanomaterials. From the TEM analysis, it is clear that almost all the Sb_2Te_3 nanomaterials are separated from each other that are due to adsorption of CTAB surfactant on the particle surface as a protective cell to prevent unwanted agglomeration. At this point we are not 100% sure about the exact growth mechanism and formation of different morphology and a detailed study will be done in near future to figure out an insight into the detailed mechanism for the formation of shape-selective Sb_2Te_3 nanomaterials. Taking two different morphologies of Sb_2Te_3 nanomaterials, we studied their activity as thermoelectric materials as discussed below.

Thermoelectric application of shape-selective Sb_2Te_3 nano materials.

In our present method we synthesized polycrystalline samples of Sb_2Te_3 nanomaterials by changing the surfactant concentration and observed two different morphologies such as dumb-bell like and chain-like shapes. The advantage of chemical routes based synthesis of the TE materials is that it can formed nanoscale object in a shorter time and decoupling electrical, thermal conductivities and reduce the thermal property through phonon scattering.[4] The dimensionless ZT values were calculated using equation: $ZT = [S^2\sigma/\kappa_{latt} + \kappa_{el}] T$, where *S* is Seebeck coefficient, σ is electrical conductivity and κ are thermal conductivity ($\kappa = \kappa_{latt} + \kappa_{el}$), which depend on the sum of the two factor, one is lattice thermal conductivity (κ_{latt}) another one is electronic thermal conductivity (κ_{el}) and T is the absolute temperature, respectively.

Antimony telluride (Sb_2Te_3) is a significant group V-VI TE material at low temperature due to its narrow-band gap and lager ZT value.[53] Antimony telluride (Sb_2Te_3) attracted considerable fundamental and technological interests for decades because of its potential applications in mini-power-generation systems and micro-coolers, CCD technology, and infrared detectors. Usually in semimetal of Sb_2Te_3 both hole and electrons are participating in the conducting mechanism. Dong et al. reported the TE property of microwave-assisted synthesized hexagonal Sb_2Te_3 nanosheets and they obtained high electrical conductivity σ ($2.49 \times 10^4\ \Omega^{-1}\ m^{-1}$), high Seebeck coefficient S (210 $\mu V\ K^{-1}$), low thermal conductivity k (0.76 $W\ m^{-1}\ K^{-1}$) and ZT of 0.58 at 420 K.[54] Sb_2Te_3 has attracted greater attention for high σ, $3.13–5.26 \times 10^5\ \Omega^{-1}\ m^{-1}$ at 300 K and low k of 1.6–5.6 $Wm^{-1}\ K^{-1}$ at 300 K of the single crystal.[55] Most recently, Zhao and co-workers reported the highest TE material of SnSe, which show ZT value 2.62 at 923 K along a particular crystallographic direction.[56] The higher ZT values of SnSe due to lower k_L and lighter elements compared to heavier $Cu_{2-x}Se$ due to effect the stronger anharmonic character of the copper-sulfide bonds.[57] Usually, due to the structural difference appeared between nanowire and bulk material, the degeneracy of carrier pocket varies significantly when a wire is orientated along different direction.[58] The electrical conductivity measurement was done with variation of temperature for dumb-bell like (a) and wire-like (b) structure as shown in Figure 6A. Electrical conductivity of Sb_2Te_3 system shows initially degenerate semiconductor behavior because conductivity decreases at starting point. The thermal condutivity of the both sample was decreasing, while increasing the temperature indicates the metallic behaviour of the Sb_2Te_3 alloy. After the temperater at 380K it stat to increase upto 400K shows typical intrinsic

behavior such that conductivity increases with increasing temperature.The increament of electrical condutivity after certain temperature may due to the thermal exicitation of carriers.[58]

The seebeck coefficient measurment of both dumb-bell like (a) and chain-like (b) structure are presented in Figure 6B. The wire-like structure showed large Seebeck coefficient value at starting temperature then while increasing the temperature, the Seebeck coefficient value was decreaing. The Seebeck coefficient decreasing at high temperature is due to increasing the electrical condutivity of the sample. The dumb-bell like structure showed Seebeck coefficient decreasing from the strating point and after 450K, it is increasing due to decrement of electrical condutivity of the sample. Chain-like Sb_2Te_3 alloys indicates a typical semiconductor behavior resulting lower Seebeck values at high temperatures. The Sb_2Te_3 nano-chain show high Seebeck coefficient while a small temperature gradient is applied to the nanomaterials compared to higher temperature. Usually Sb_2Te_3 nanomaterials are semi-metallic in nature where both the hole and electrons are participating in the conducting mechanism. Lin et al. reported that the bismuth nanowires have a significantly improved Seebeck coefficient value compared to its bulk material because bulk bismuth is a semimetal and a semimetal-to-semiconductor transition is expected to occur below a critical nanowire size (ca. 50 nm) due to quantum-confinement properties.[59] The Seebeck coefficient measurement shows the sudden increment with decrease in the temperature region ~ 400-450K may be attributed due to structural phase transition that also compared with earlier analysis.[60]

The total thermal condutivty (κ) value of each Sb_2Te_3 nanomatrials was evaluated from the thermal diffusivity α, heat capacity C_p, and smaple density ρ, based on the relationship $\kappa = \alpha C_p \rho$. Figure 7A indicates the comparison of total thermal conductivity values of the both Sb_2Te_3 nanomaterials with different temperature.The thermal conductivity of both sample was decreasing from strating point and the k value of dumb-bell like structure ~ 0.84 W m^{-1} K^{-1} and chain-like structure ~ 0.67 W m^{-1} K^{-1} at 440K. Due to Umklapp scattering (phono-phonon scattering), κ value decrease at high temperatures for both Sb_2Te_3 samples. From the earlier report, the thermal conductivity of the Bi hetero-structure nanowires with small diameters (20–25 nm) shows 0.55 W m^{-1} K^{-1} at 300 K and Bi bulk counterpart shows 8 W m^{-1} K^{-1} at same temperater.[61] The nanowires shows the k value 15 times lower than that of the bulk materials which is probably due to the increased phonon scattering effect. Compared to dumb-bell like structure, chain-like structure give better thermal conducting behavior which and consequently increasing the ZT value.

The dimensionless ZT value of Sb_2Te_3 nanomaterial's analyzed with respect to change in temperature as shown in Figure 7B. From the analysis we got efficency of the dumb-bell like (a) structure having 0.01 at nearly 450K and chain-like (b) structure is ~ 0.1 at 300K. We plot the ZT value of two different samples at different temperature because they gave maximum ZT at that temperature only. In case of dumb-bell like morphology, it showed a ZT value of 0.004 at 300K. Compared to dumb-bell like structure, chain-like structure having more ZT value because vicinal degeneracy decreases when a wire becomes slimmer due to the quantum confinement Effect.[57] From electrical conductivity measurement, chain-like structure shows good electrical performance even at high temperature. The Seeback coefficient measurement showed that in case of chain-like structure, it decreasing initially due to increase in the electrical performance of Sb_2Te_3. So compared to dumb-bell like structure, chain-like structure giving less thermal conducting behaviour and heat loss is also less in the case of chain-like structure. Hence, the chain-like structure fulfil all the criteria like increment of electrical conductivity at the same time decreasing the thermal conductivity and due to this dual nature results enhance efficiency of the Sb_2Te_3 chain-like nanomaterial. Hicks and Dresselhaus reported that low dimensional materials give better ZT value compares to their bulk ones due to low-dimensional effects on both charge carriers and lattice waves.[62,63] As reported earlier, nanostructure materials having great advantage to efficiently reduce the lattice thermal conductivity via the effective phonon scattering present at the interface between boundaries of the nanograins in the rough surfaces area of the nanowires an it enhance the ZT value.[64,65] The same group reported the ZT value of different size nanowires and it show the 10 nm size Sb_2Te_3 wire has a larger maximal ZT value compared to 5 nm because slim wire and low dimensional TE material will always give larger ZT value. Zhang et al. reported that control the growth direction of the nanowire will increase the ZT value due to increasing the number of near degenerate conduction (valence) sub-bands induced by quantum confinement.[57] Hence, by analyzing all parameters we observed that chain-like Sb_2Te_3 nanomaterials give better performance compared to dumb-bell like structure. Finally, we checked the morphology of the samples after plasma sintering process to test if there is any change due to the sintering. Figure 8, A-D shows the TEM images of the dumb-bell like (A-B) and chain-like (C-D) Sb_2Te_3 nanomaterials after sintering process. Figure 8, A and B shows the low and high magnified TEM images which shows that the originally dumb-bell like morphology are compacting and fused together to form aggregated dumb-bell like shapes due to applying temperature and pressure during sintering process. Similarly, Figure 8, C and D shows the the low and high magnified TEM images which also

showed that the originally chain-like morphology are fused, aggregated and generated distorted longer chain-like shapes. Other than TEM, we also did the XRD and EDS analysis of the post sintering samples. Figure S-4 (online SI section) shows the camera images of the post sintering samples (A and B), XRD analysis (Figure S-4C) and EDS analysis (Figure S-4D). Post sintering XRD patterns of the Sb_2Te_3 nanomaterials shown in Figure S-4C where pattern a denote for aggregated dumb-bell like morphology whereas pattern b is of aggregated chain-like morphology. Both the patterns gave almost identical XRD features like before sintering but in case of aggregated chain-like morphology, the (014) crystal plane showing high intensity compare to aggregated dumb-bell like morphology. Moreover, after sintering, the peak intensity of both XRD patterns reduced but the original peak positions remained same. The change in intensity might be due to morphology changes triggered by particle-particles fusion, compacting and un-even grain growth. Figure S-4D shows the EDS analysis of Sb_2Te_3 nanomaterials after sintering which gave almost similar EDS pattern like before. As an example, we have used aggregated dumb-bell like morphology here for EDS analysis although other morphology also shows similar EDS spectrum (not shown here). At this moment we are not fully sure about the exact reason of change of particles morphology due to sintering but it is reasonable to assume that it might be due to applying temperature, pressure which induces particles particle fusion, compacting and increasing density during sintering process.

Conclusion

In summary, a low temperature route has been employed for the formation of shape-selective Sb_2Te_3 nanomaterials within a short reaction time. Dumb-bell like and chain-like Sb_2Te_3 nanomaterials are formed by the reaction of Te metal powder with $SbCl_3$ salt in the presence of alkaline 2,7-DHN in CTAB micelle media at 80 °C temperature. The size and shape of materials can be easily tuned just by changing the molar ratio of the surfactant to metal salts and controlling the other reaction parameters. The size of the middle part of the dumb-bell like shapes are ~ 15 ± 1 nm, and the length ~ 50 ± 7 nm while the diameter of the chains is ~ 125 ± 7 nm. The electronic property, thermal stability and specific growth mechanism for the formation of different shapes were elaborated in detail. Among the two different morphologies, the chain-like morphology gives a better thermoelectric figure of merit (ZT) value compare to dumb-bell like morphology at 300K. The higher ZT value of chain-like morphology is due to reduction of the lattice thermal conductivity via the effective

phonon scattering that present at the interface between boundaries of the nanograins and in the rough surfaces of the nano-chains. The maximum ZT temperature moves significantly to the high temperature zone indicating that the shape-selective Sb_2Te_3 nanomaterials have potential application in future power generation, deep-space probes and in gas fuelled generators in remote locations. Moreover, currently we are trying to modify the morphology of the material by introducing some foreign materials to increase the ZT value significantly.

Supporting Information (SI) Available: The detailed instrument specifications are provided. The detailed analysis related to UV-Vis study, Energy Dispersive X-ray Spectroscopy (EDS) and thermal analyses (TGA-DTA) and their corresponding Figures as Figures S-1 to S-3 are given. The figure related to camera image, XRD pattern and EDS analysis (as figure S-4) of Sb_2Te_3 nanomaterials after post plasma sintering process is given. This material is available free of charge via the Internet at http://pubs.rsc.org.

Acknowledgement: S K, U N and S R Ede wish to acknowledge Dr. Vijayamohanan K. Pillai, Director, and Dr. M. Jayachandran, HOD, ECMS division, CSIR-CECRI for their continuous support and encouragement. S. R. Ede wishes to acknowledge council of scientific and industrial research (CSIR) for JRF fellowship and U. Nithiyanantham wishes to thank CSIR-CECRI for research-intern fellowship. We also wish to acknowledge Mr. S Anantharaj, CSIR-JRF, ECMS division, CSIR-CECRI for proof reading the entire MS. The institute start up funding (Project number IHP 0067, DU No 5, old number OLP-0067), support from the Central Instrumental Facility (CIF) and help from Mr. V. Prabu (FE-SEM in-charge, CIF), CSIR-CECRI, Karaikudi are greatly appreciated.

References.

(1) D. M. Rowe, (ed.) *CRC Handbook of Thermoelectrics*(CRC, Boca Raton, 1995).

(2) L. E. Bell, *Science*, 2008, **321**, 1457.

(3) H. Zhang and D. V. Talapin, *Angew. Chem. Int. Ed*., 2014, **53**, 9126.

(4) C. Kim, D. H. Kim, H. Kim and J. S. Chung, *ACS Appl. Mater. Interfaces.*, 2012, **4**, 2949.

(5) C. Wood, *Rep. Prog. Phys*., 1988, **51**, 459.

(6) D. M. Rowe, *CRC Handbook of Thermoelectrics*, CRC Press, London, 1995.

(7) C. Kittel, Introduction to Solid State Physics, 8. Aufl., Wiley, New York, 2005.

(8) G. S. Nolas, J. Sharp and H. J. Goldsmid, *Thermoelectrics: Basic principles and new materials developments*; Springer: New York, 2001.

(9) L. D. Hicks and M. S. Dresselhaus, *Phys. Rev. B: Condens. Matter*, 1993, **47**, 16631.

(10) R. Venkatasubramanian, E. Silvola, T. Colpitts, and B. O. Quinn, *Nature*, 2001, **413**, 597.

(11) Y. Q. Cao, X. B. Zhao, T. J. Zhu, X. B. Zhang and J. P. Tu, *Appl. Phys. Lett*., 2008, **92**, 143106.

(12) B. Poudel, Q. Hao, Y. Ma, Y. C. Lan, A. Minnich, B. Yu, X. Yan, D. Z. Wang, A. Muto, D. Vashaee, X. Y. Chen, J. M. Liu, M. S. Dresselhaus, G. Chen and Z. F. Ren, *Science*, 2008, **320**, 634.

(13) H. Zou, D. M. Rowe and S. G. K. Williams, *Thin Solid Films*, 2002, **408**, 270.

(14) D. M. Rowe, *Thermoelectrics Handbook: Macro to Nano*, CRC Press, New York, 2006, Section III, (Chapter 27), p 16.

(15) J. H. Kim, Y. C. Jung, S. H. Suh and J. S. Kim, *J. Nanosci. Nanotechnol*., 2006, **6**, 3325.

(16) Y. Kim, A. DiVenere, G. K. L. Wong, J. B. Ketterson, S. Chao and J. R. Meyer, *J. Appl. Phys*.,2002, **91**, 715.

(17) P. Fan, Z. H. Zheng, G. X. Liang, D. P. Zhang and X. M. Cai, *J. Alloys and Compounds* 2010, **505,** 278.

(18) T. C. Patel and P. G. Patel, *Mater. Lett*., 1984, **3**, 46.

(19) N. G. Patel and P. G. Patel, *J. Mater. Sci*., 1991, **26**, 2543.

(20) L. W. da Silva, M. Kaviany and C. Uher, *Appl. Phys*., 2005, **97**, 114903.

(21) W. Shi, J. Yu, H. Wang and H. Zhang, *J. Am. Chem. Soc*.,2006, **128**, 16490.

(22) W. Shi, L. Zhou, S. Song, J. Yang and H. Zhang, *Adv. Mater*.,2008, **20**, 1892.

(23) Q. L. Yuan, Q. L. Nie and D. X. Huo, *Curr. Appl. Phys*., 2009, **9**, 224.

(24) W. Zhu, J. Y. Yang, D. X. Zhou, C. J. Xiao and X. K. Duan, *Electrochim. Acta*, 2008, **53**, 3579.

(25) J. S. Lee, S. Brittman, D. Yu and H. Park, *J. Am. Chem. Soc*., 2008, **130**, 6252.

(26) W. Wang, B. Poudel, J. Yang, D. Z. Wang and Z. F. Ren, *J. Am. Chem. Soc*., 2005, **127**, 13792.

(27) C. Jin, G. Zhang, T. Qian, X. Li, and Z. Yao, *J. Phys. Chem. B*, 2005, **109**, 1430.

(28) S. S. Garje, D. J. Eisler, J. S. Ritch, M. Afzaal, P. O'Brien and T. Chivers, *J. Am. Chem. Soc*., 2006, **128**, 3120.

(29) G. –H .Dong, Y. –J. Zhu and L. –D .Chen.*J. Mater. Chem*., 2010, **20**, 1976.

(30) D. Pinisetty and R. V. Devireddy, *Acta Mater*., 2010, **58**, 570.

(31) A. G. Cullis and P. A. Midgley, *Microscopy of Semiconducting Materials 2003, Royal Microscopical Society*, Great Britain, pp 601–606.

(32) S. Kundu, S. Lau, and H. Liang, *J. Phys. Chem. C*, 2009, **113**, 5150.

(33) S. Kundu, *Phys. Chem. Chem. Phys*., 2013, **15**, 14107.

(34) U. Nithiyanantham, S. R. Ede, and S.Kundu, *J. Mater. Chem. C*, 2014, **2**, 3782.

(35) S. Kundu, M. D. Mukadam, S. M. Yusuf and M. Jayachandran, *Cryst. Eng. Commun*., 2013, **15**, 482.

(36) U. Nithiyanantham, A. Ramdoss, S. R. Ede and S. Kundu, *Nanoscale*, 2014, **6**, 8010.

(37) S. Shi, M. Cao and C. Hu, *Cryst. Growth Des*., 2009, **9**, 2057.

(38) G. Gupta and J. Kim, *Dalton Trans*., 2013, **42**, 8209.

(39) S. R. Ede, U. Nithiyanantham and S. Kundu, *Phys. Chem .Chem. Phys*., 2014, **16**, 22723.

(40) S. Kundu, L. Peng and H. Liang, *Inorg. Chem*., 2008, **47**, 6344.

(41) S. Kundu, K. Wang and H. Liang, *J. Phys. Chem. C*, 2009, **113**, 18570.

(42) S. Kundu and H. Liang, *Langmuir*, 2010, **26**, 6720.

(43) S. Kundu, K. Wang, S. Lau and H. Liang, *J. Nanopart. Res*., 2010, **12**, 2799.

(44) S. Kundu, D. Huitink and H. Liang, *J. Phys. Chem.C*, 2010, **114**, 7700.

(45) A. Pal and T. Pal, *J. Raman Spectrosc*., 1999, **30**, 199.

(46) S. Kundu, K. Wang and H. Liang, *J. Phys. Chem. C*, 2009, **113**, 134.

(47) S. Kundu, S. Panigrahi, A. Pal, S. Basu, S. Praharaj, S. K. Ghosh and T. Pal, *Nanotechnology*, 2007, **18**, 75712.

(48) S. Kundu and H. Liang, *Langmuir*, 2008, **24**, 9668.

(49) D. Majumdar, A. Singha, P. K.Mondal and S. Kundu, *ACS Appl. Mater. Interfaces*, 2013, **5**, 7798.

(50) J. M. Petroski, Z. L. Wang, T. C. Green and M. A. El-Sayed, *J. Phys. Chem. B*,1998,**102**, 3316.

(51) N. R. Jana, L. Gearheart and C. J. Murphy, *J. Phys. Chem. B*, 2001, **105**, 4065.

(52) Y. Song, R. M. Garcia, R. M. Dorin, H. Wang, Y. Qiu, E. N. Coker, W.A Steen, J. E. Miller and J. A. Shelnutt, *Nano Lett*., 2007, **7**, 3650.

(53) D. Pinisetty and R. V. Devireddy, *ActaMater*., 2010, **58**, 570.

(54) G. H. Dong, Y. J. Zhu and Li-Dong Chen, *J. Mater. Chem*., 2010, **20**, 1976.

(55) D. M. Rowe, *Thermoelectrics Handbook: Macro to Nano*, CRC Press, New York, 2006, Section III, (Chapter 27), p 16.

(56) Y. He, T. Day, T. Zhang, H. Liu, X. Shi, L. Chen and G. J. Snyder, *Adv. Mater*., 2014, **26**, 3974.

(57) G. R. Zhang and Z. Zeng, *Journal of Physics: Conference Series.*, 2009, **193**, 012110.

(58) L. D. Zhao, S. H. Lo, Y. Zhang, H. Sun,G. Tan, C. Uher, C. Wolverton, V. P. Dravid and M. G. Kanatzidis, *Nature*, 2014, **508**, 373.

(59) Y. M. Lin, X. Z. Sun and M. S. Dresselhaus, *Phys. Rev.B: Condens. Matter Mater. Phys*., 2000, **62**, 4610.

(60) J. Pei, G. Chen, D. Jia, Y. Yu, J. Sun, H. Xu and Z. Qiu, *New J. Chem.*, 2014, **38**, 59.

(61) G. Zhang, Q. Yu and X. Li. *Dalton Trans.*, 2010, **39**, 993.

(62) L. D. Hicks, M. S. Dresselhaus, *Phys. Rev. B*, 1993, **47**, 12727.

(63) L. D. Hicks, M. S. Dresselhaus, *Phys. Rev. B*, 1993, **47**, 16631.

(64) A. Hochbaum, R. Chen, R. D. Delgado, W. Liang, E. C. Garnett, M. Najarian, A. Marumdar and P. Yang, *Nature*, 2008, **451**, 163.

(65) T. Markussen, A. P. Jauho and M. Brandbyge, *Phys. Rev. B: Condens. Matter Mater. Phys*., 2009, **79**, 035415.

Figure Captions:

Figure 1. Transmission Electron Microscopy (TEM) image of the shape-selective Sb_2Te_3 nanomaterials. Figure 1, a-c shows the TEM images of dumb-bell like morphology and Figure 1, d-f shows the TEM image of the chain-like morphology at low and high magnification. The inset of Figure 1c and Figure 1f shows the corresponding selected area electron diffraction (SAED) pattern which speaks that the particle are crystalline in nature.

Figure 2. Field-emission scanning electron microscopy (FE-SEM) images of the Sb_2Te_3 nanomaterials. Figure 2, a and b shows FE-SEM images for dumb-bell like shape and Figure 2, c and d shows images of chain-like morphology at different magnification.

Figure 3. The X-ray diffraction (XRD) pattern of the dumb-bell like (curve A) and chain-like (curve B) Sb_2Te_3 nanomaterials.

Figure 4. X-ray photoelectron spectroscopic (XPS) analysis of Sb_2Te_3 nanomaterials. In Figure 4, 'A' indicate the survey spectrum and 'B-F' indicates the high resolution scan for Sb (3d) ,Te (3d), Te (4d), O (1s), and C (1s) respectively.

Figure 5. The Fourier-transform infrared (FT-IR) spectra of only CTAB (curve a) and CTAB bound Sb_2Te_3 nanomaterials (curve b) in the wavenumber range 400-4000 cm^{-1}.

Figure 6. Thermoelectric behaviour of the synthesized dumb-bell like (a) and chain-like (b) Sb_2Te_3 nanomaterials. (A) Electrical conductivity measurement and (B) Seebeck coefficient analysis with change in temperature.

Figure 7. Thermoelectric behaviour of the synthesized dumb-bell like (a) and chain-like (b) Sb_2Te_3 nanomaterials. (A) Thermal conductivity measurement; (B) Figure of merit (ZT) value with change in temperature.

Figure 8. A, B and C, D shows the low and high magnified TEM images of aggregated dumb-bell like and aggregated chain-like morphology after sintering process.

Table 1: The detailed final concentrations of all the reaction parameters, time of reaction, particles size, shape etc. are summarized.

Scheme 1. The schematic presentation of the overall preparation process for the formation of Sb_2Te_3 nanomaterials on CTAB micellar media.

Scheme 2. The working principal of TE system was schematically shown in Scheme 2.

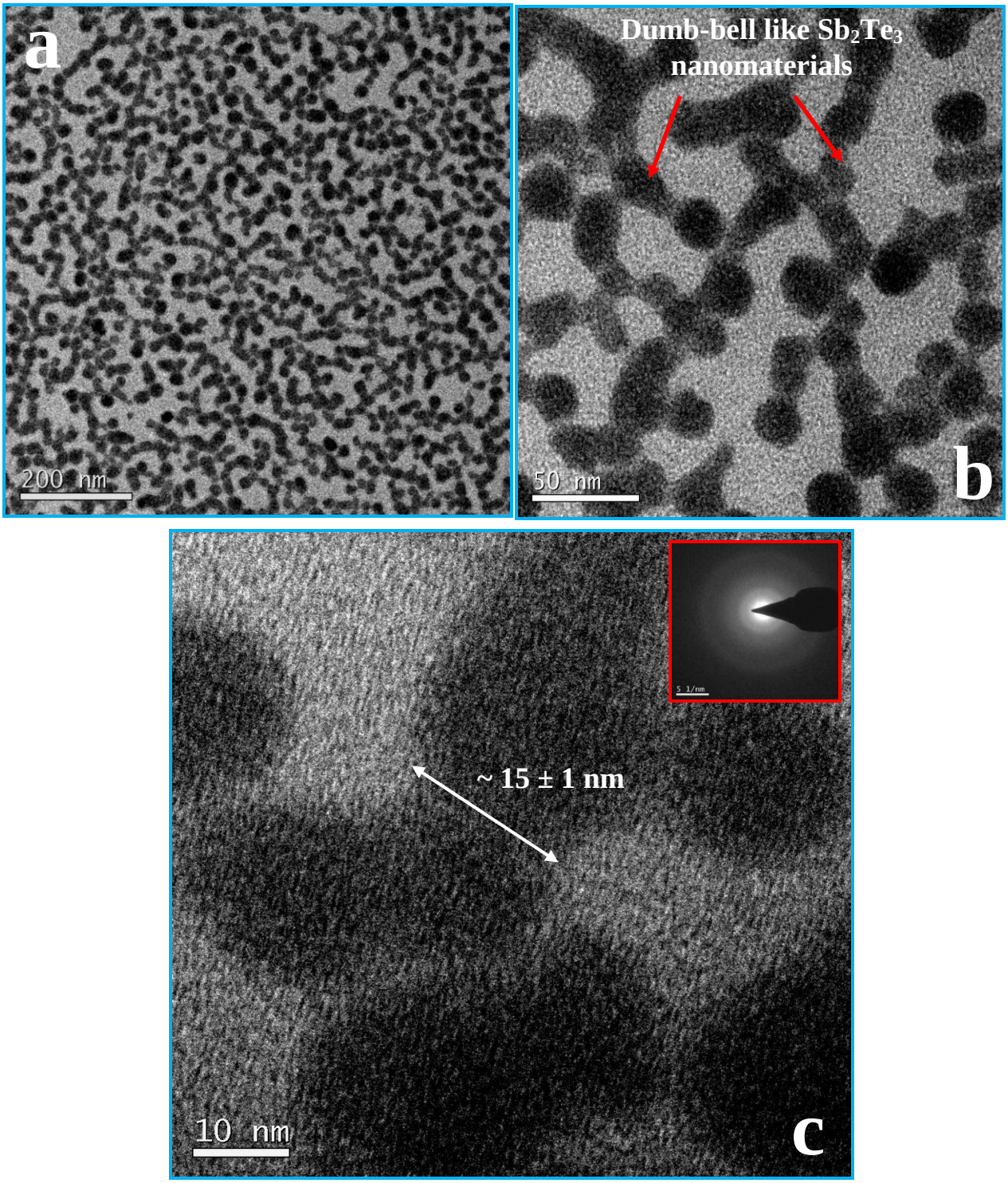

Figure 1, a-c

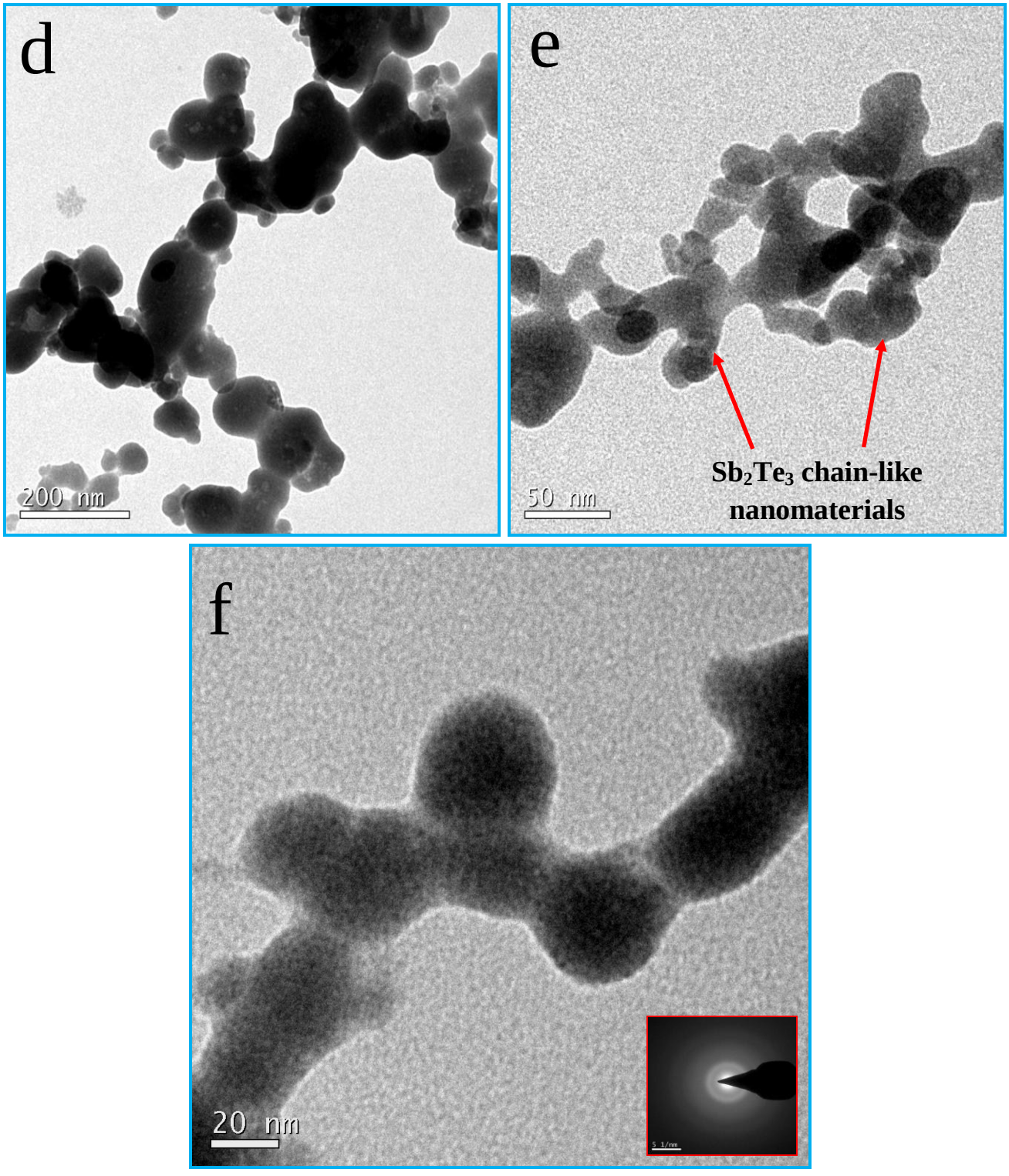

Figure 1, d-f

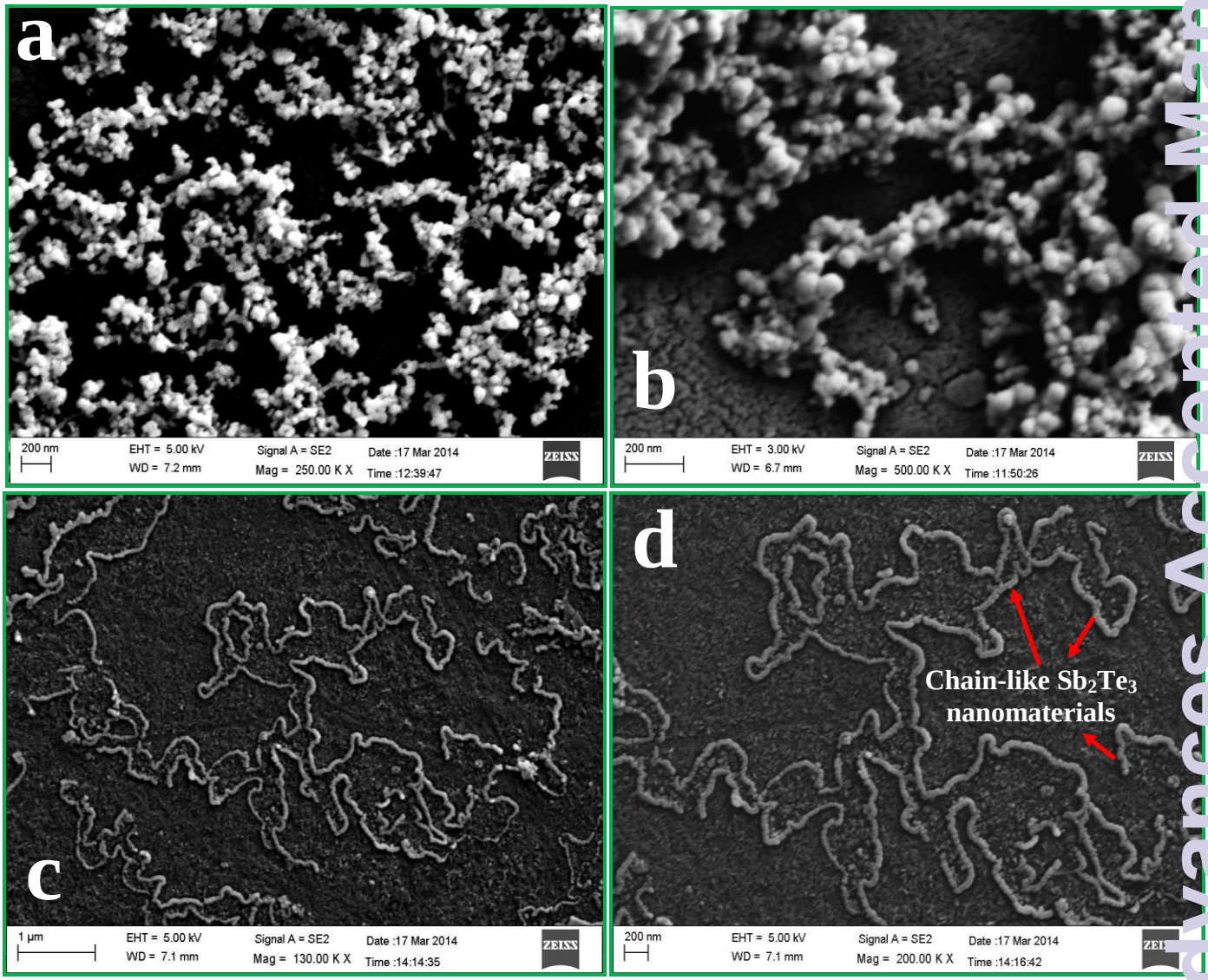

Figure 2, a-d

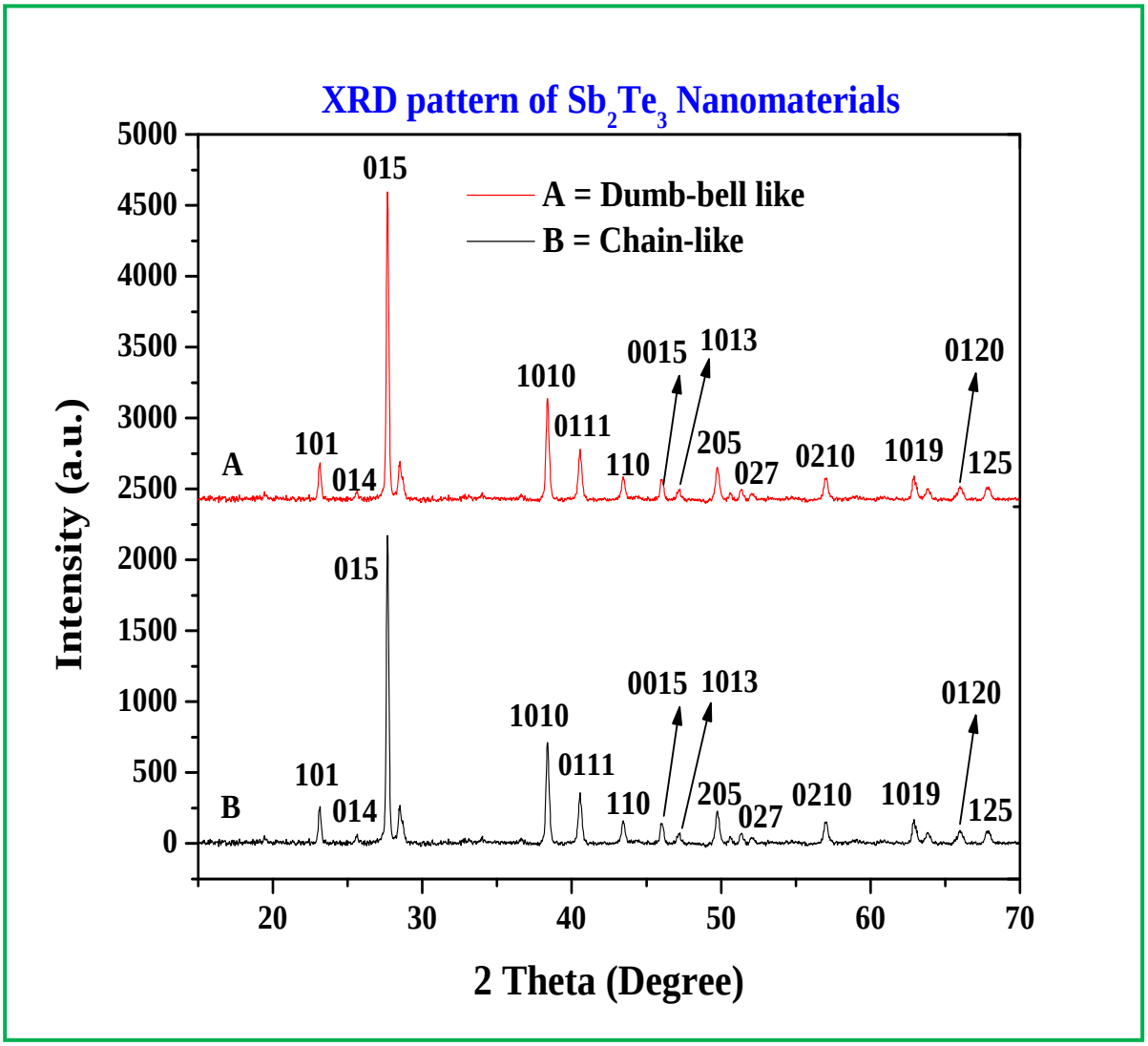

Figure 3

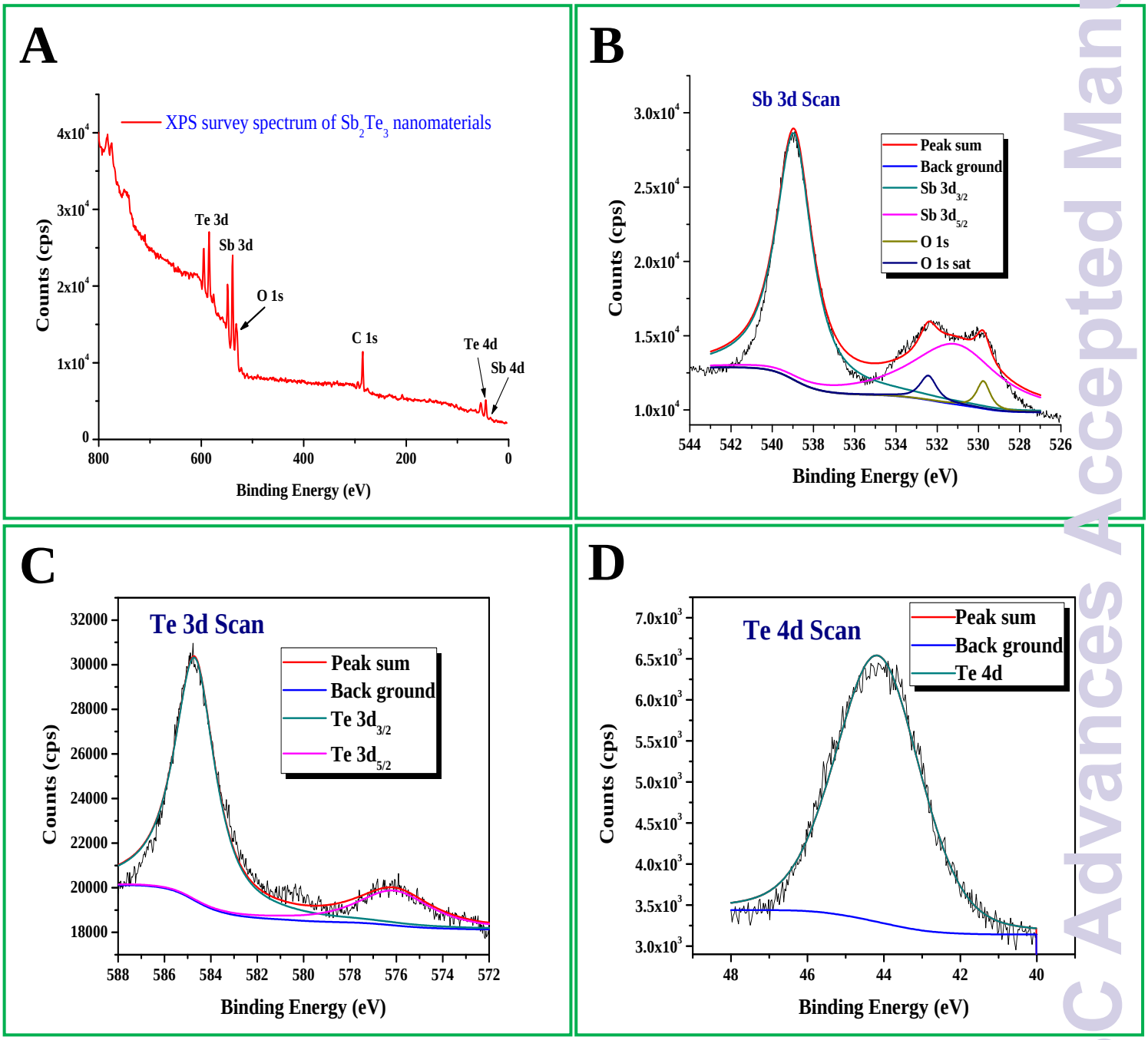

Figure 4, A-D

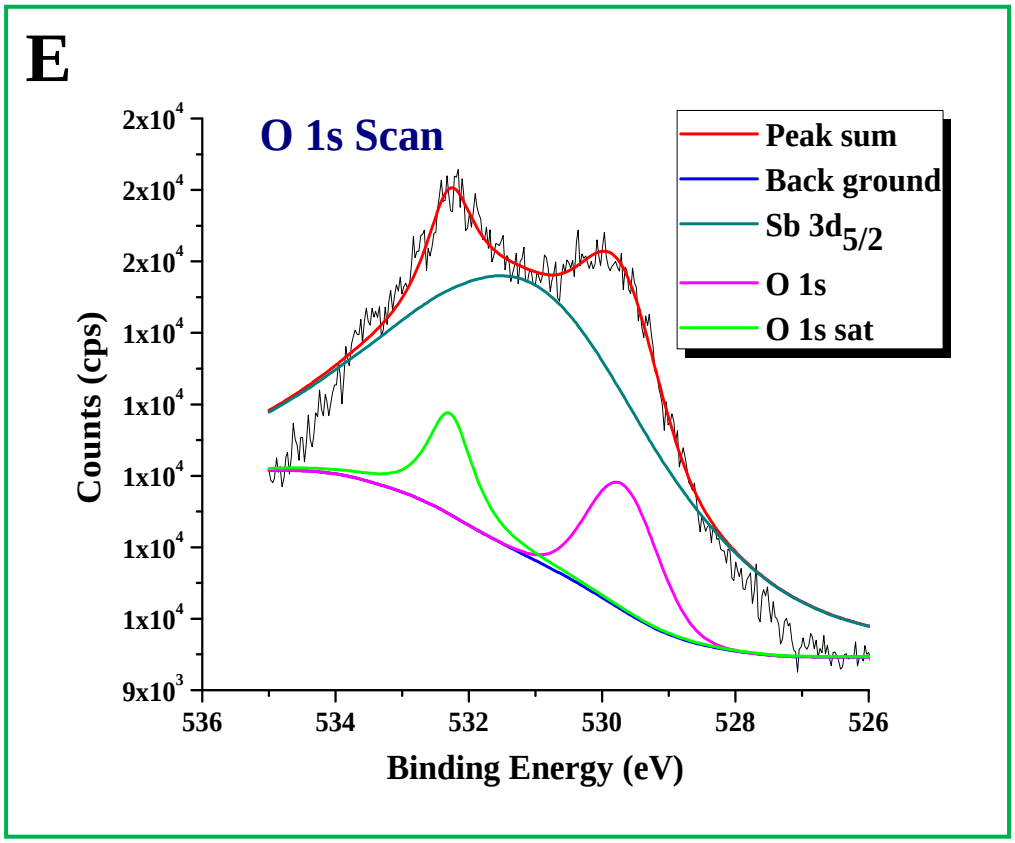

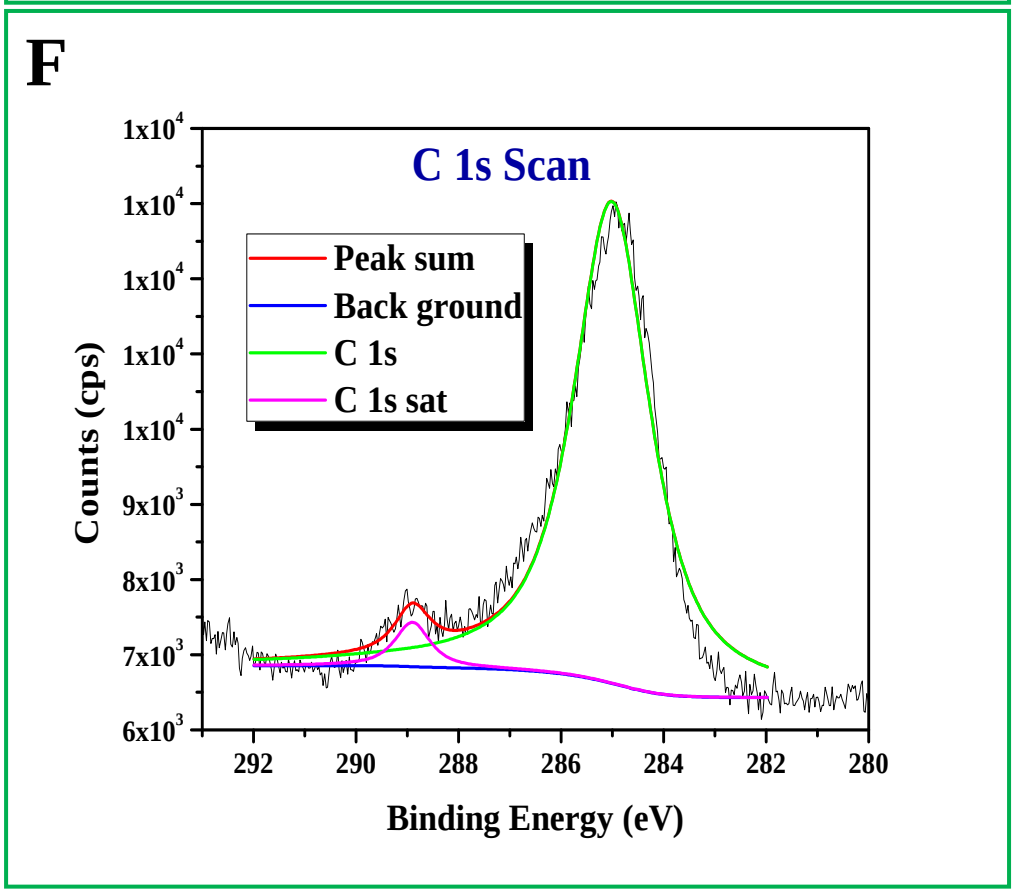

Figure 4, E-F

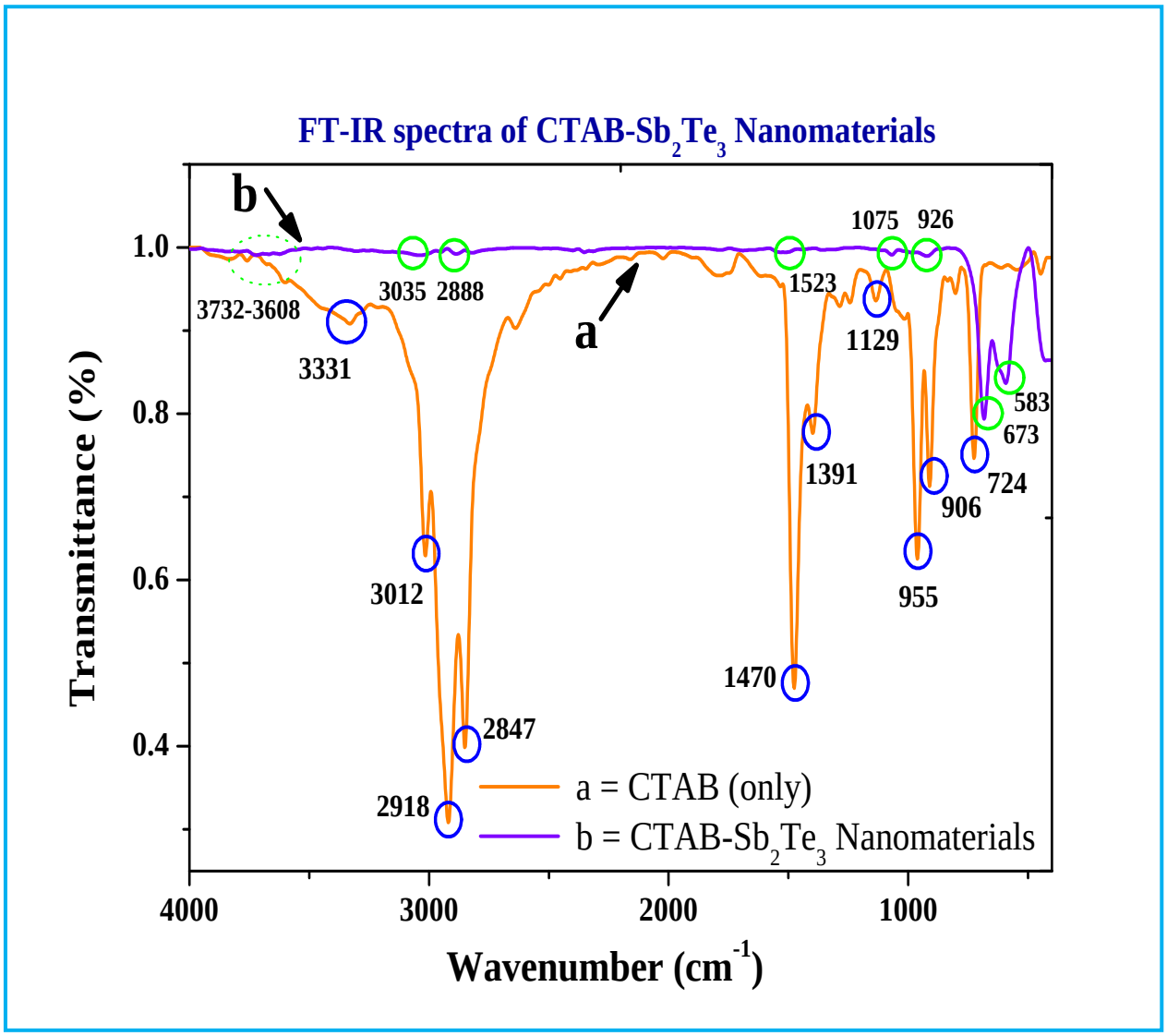

Figure 5

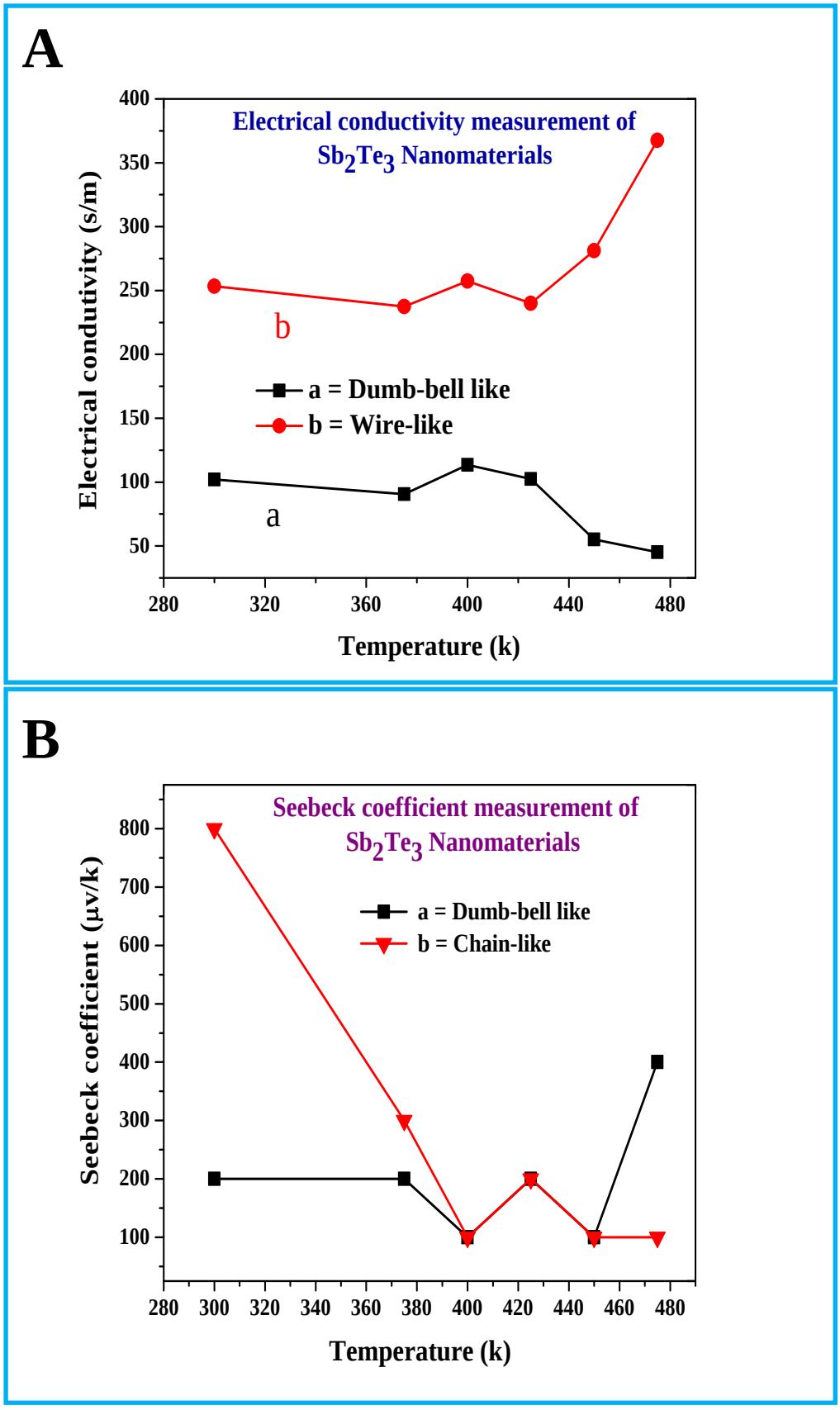

Figure 6, A-B

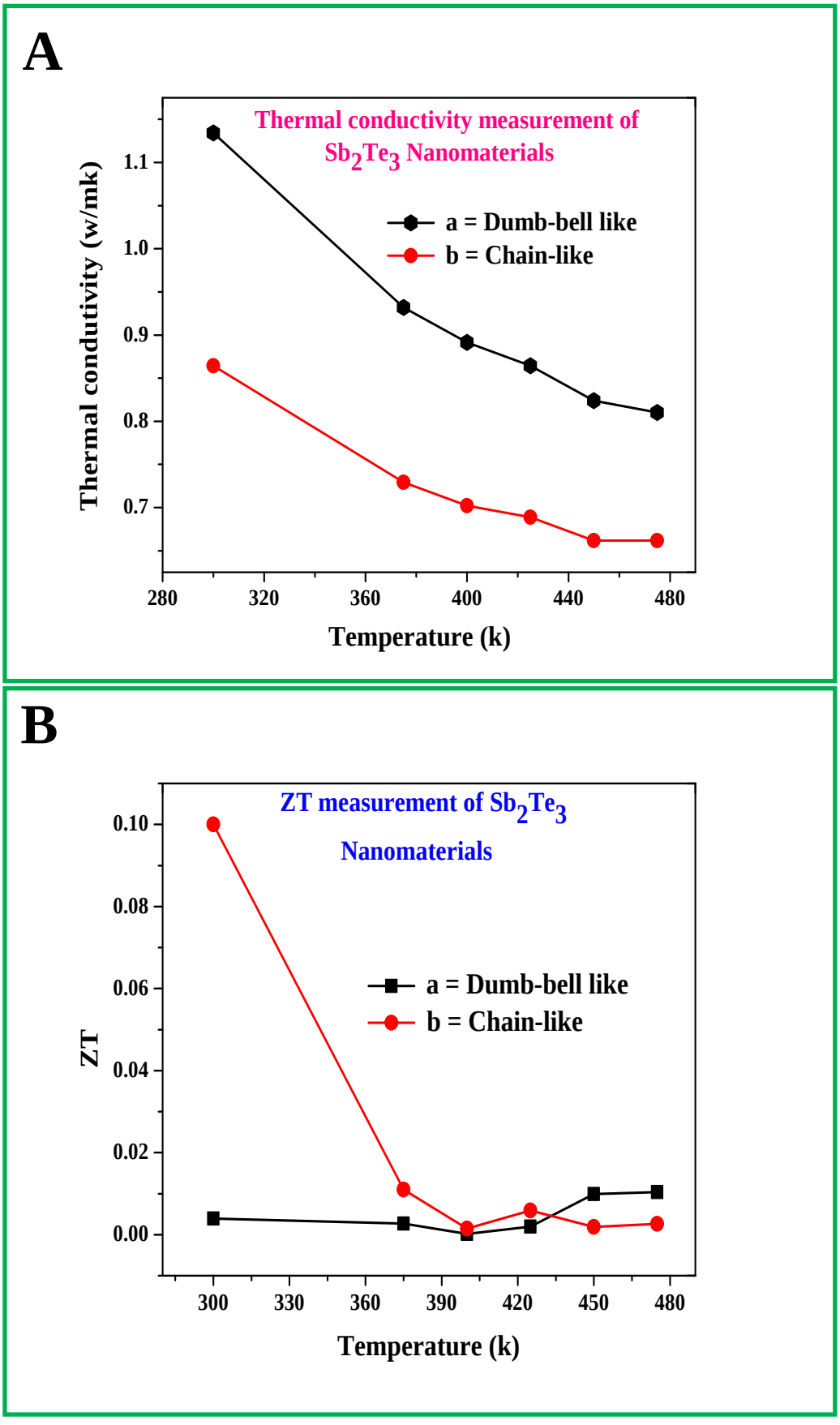

Figure 7, A-B

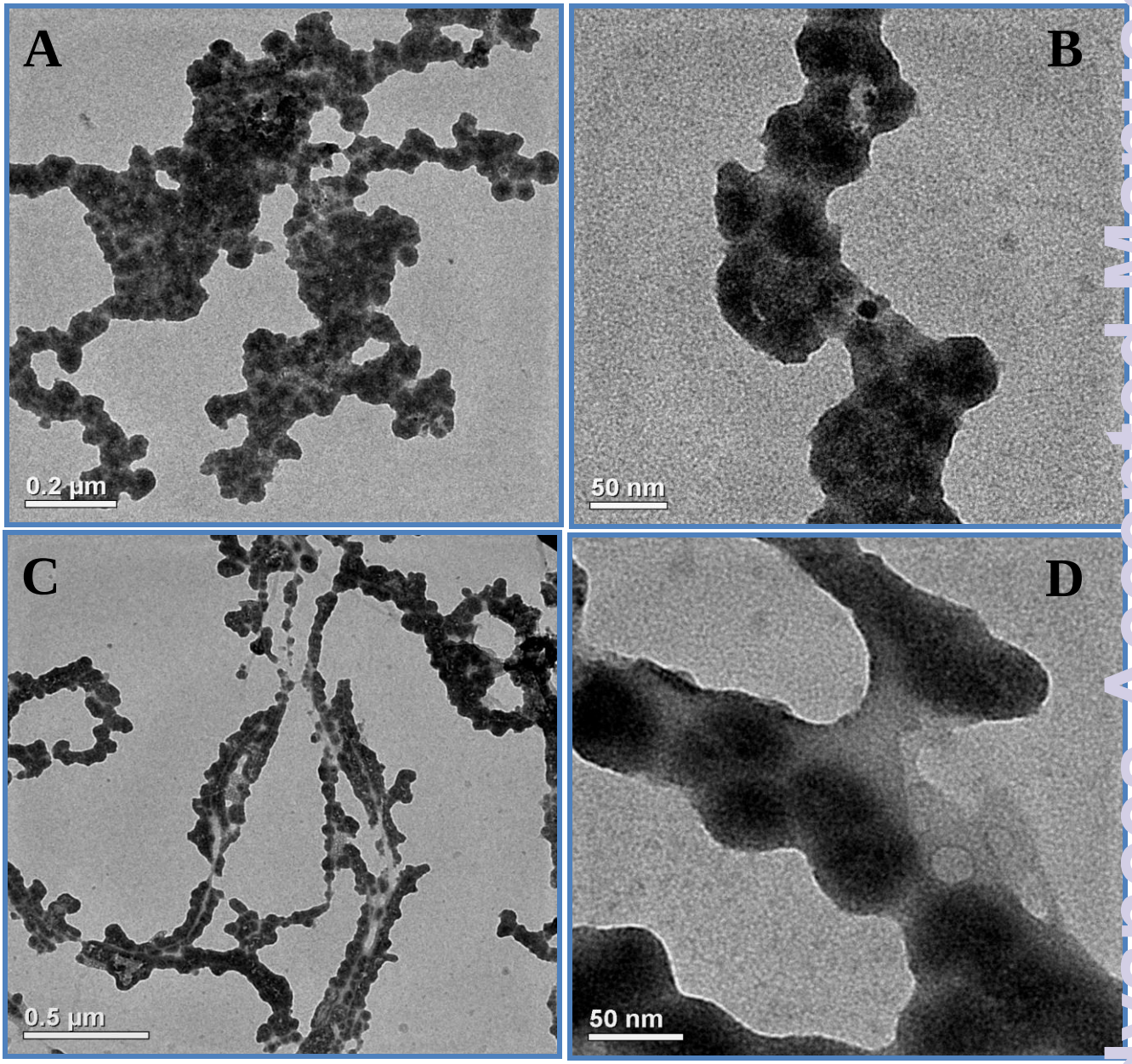

Figure 8, A-D

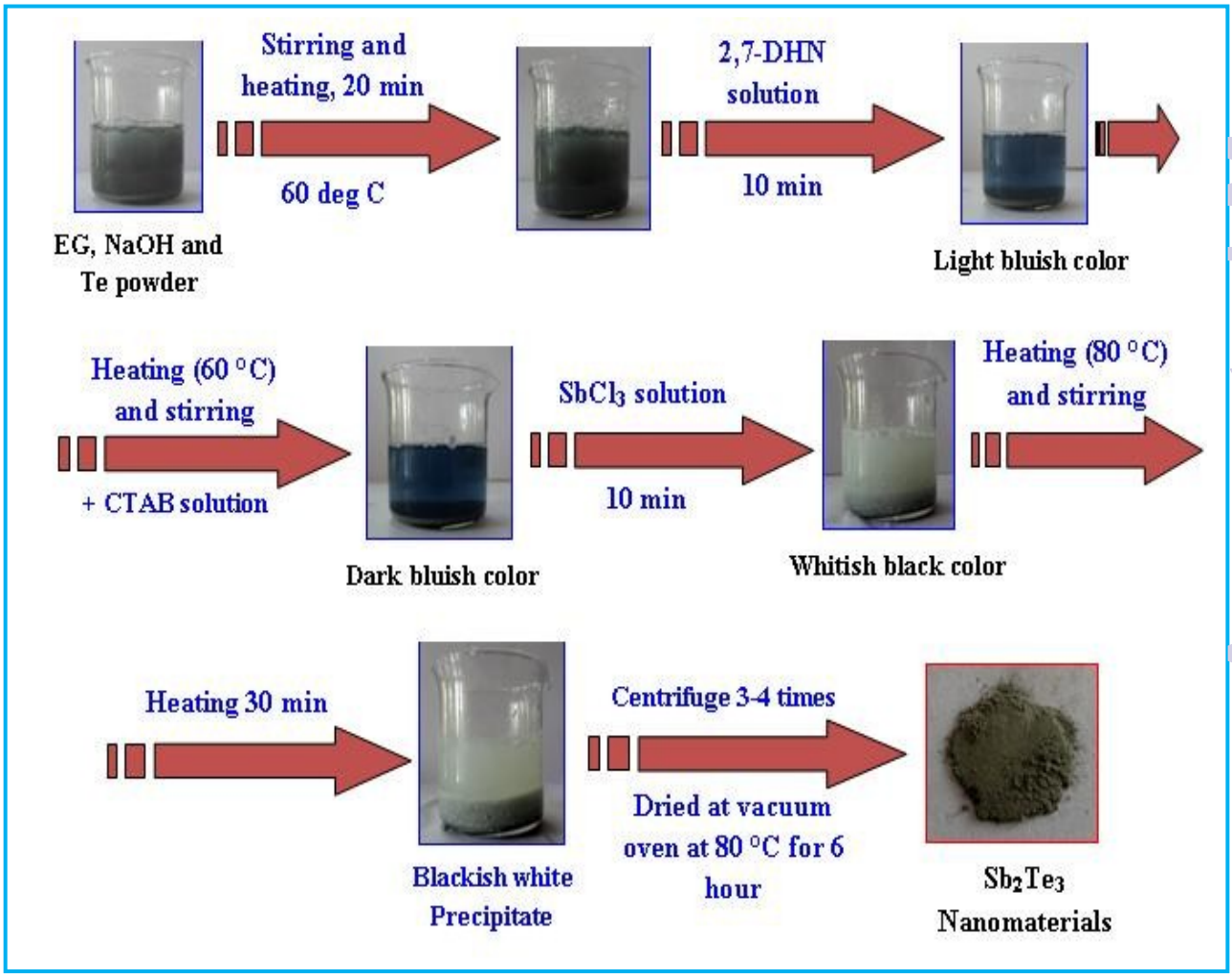

Scheme 1

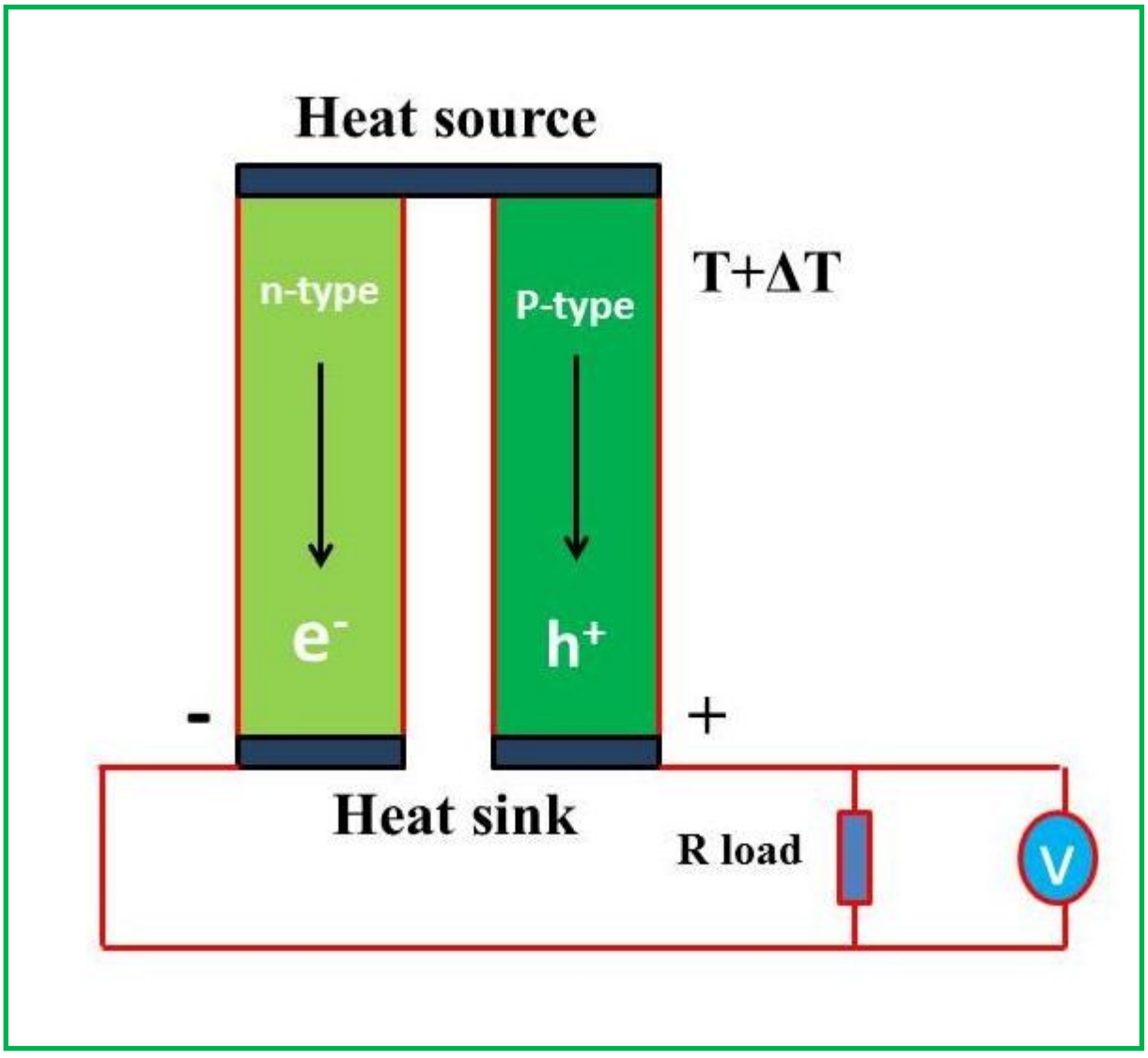

Scheme 2

Set No.	Final conc. of CTAB (M)	Final conc. of Sb(III) Chloride solution (M)	Amount of Te metal powder (gm)	Final conc. of 2,7-DHN (M)	Final conc. of NaOH (M)	Color of the solution	Average particles size (nm)	Shape of the particles
1	5.4×10^{-2}	4.58×10^{-2}	0.6	1.25×10^{-2}	0.1	Whitish yellow color	Middle ~ 15 ± 1 nm; Total length ~ 50 ± 7 nm.	Dumb-bell like
2	5.4×10^{-4}	4.58×10^{-2}	0.6	1.25×10^{-2}	0.1	Whitish yellow color	Diameter ~ 125 ± 7 nm; Length ~ 1.2 - 1.5 µm.	Chain-like

Table 1

Table of Contents

Low Temperature, Shape-selective Formation of Sb_2Te_3 Nanomaterials and their Thermoelectric Applications

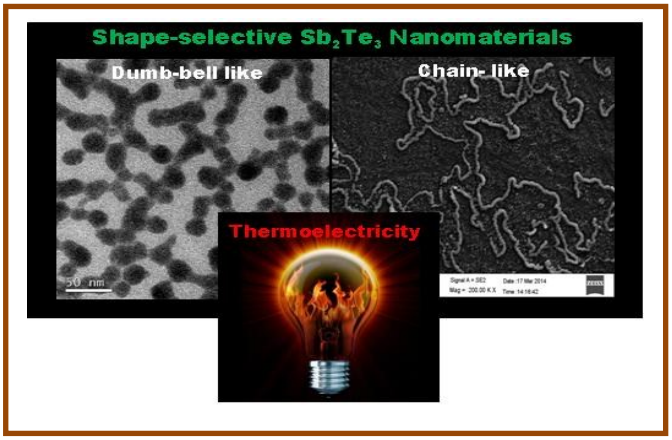

ABSTRACT

Thermoelectric properties of shape-selective Sb_2Te_3 nanomaterials which synthesized at a low temperature within a short reaction time have been reported.